J. Fluid Mech. (2023), *vol*. 954, A11, doi:10.1017/jfm.2022.959

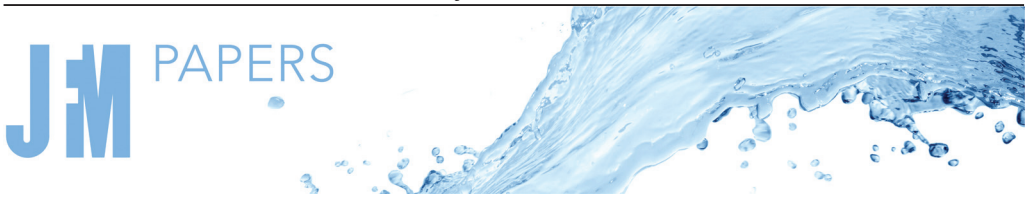

Theoretical analysis for bedload particle deposition and hop statistics

Zi Wu[1,2,†], **Weiquan Jiang**[1,2,†], **Li Zeng**[3] **and Xudong Fu**[1,2,†]

[1]Department of Hydraulic Engineering, Tsinghua University, Beijing 100084, PR China

[2]State Key Laboratory of Hydroscience and Engineering, Tsinghua University, Beijing 100084, PR China

[3]State Key Laboratory of Simulation and Regulation of Water Cycle in River Basin, China Institute of Water Resources and Hydropower Research, Beijing 100038, PR China

(Received 17 April 2022; revised 24 September 2022; accepted 6 November 2022)

Understanding the statistics of bedload particle motions is of great importance. To model the hop events which are defined as trajectories of particles moving successively from the start to the end of their motions, recently, Wu *et al.* (*Water Resour. Res.*, vol. 56, 2020, p. e2019WR025116) have successfully performed individual-based simulations according to the Fokker–Planck equation for particle velocities. However, analytical solutions are still not available due to (i) difficulties in treating the velocity-dependent diffusivity, and (ii) a knowledge gap in incorporating the termination of particle motions for the equation. To tackle the above-mentioned challenges, we first specify a Robin boundary condition representing the deposition of particles. Second, for analytical solutions of hop statistics, a variable transformation is devised to deal with the velocity-dependent diffusivity. The original bedload transport problem is thus found to be governed by the classic equation for the solute transport in tube flows with a constant diffusivity after the transformation. Finally, through solving the spatial and temporal moments of the governing equation, we investigate the influence of the deposition rate on three key characteristics of particle hops. Importantly, we have related the deposition rate to the mean travel times and hop distances, enabling a direct determination of this physical parameter based on measured particle motion statistics. The analytical solutions are validated by experimental observations with different bedload particle diameters and transport conditions. Based on the limited experimental datasets, the deposition frequency is shown to decrease as the shear stress increases when the flow rate is not small.

Key words: sediment transport, dispersion

† Email addresses for correspondence: wuzi@tsinghua.edu.cn, wqjiang@pku.edu.cn, xdfu@tsinghua.edu.cn

1. Introduction

As a specific form of sediment transport, bedload transport describes the movement of relatively coarse particles adjacent to the surface of the streambed under different motions of rolling, sliding and saltation. Due to the near-bed turbulence, complex fluid–particle interactions and particle–bed collisions, bedload particle motions are inherently stochastic (Furbish *et al.* 2012*a*; Ancey 2020), with the probability theory serving as a basic tool for insightful investigations. The probability description of bedload transport has since inspired intense and ever-growing research interest, stemming from the pioneering work of Einstein (1936, 1942, 1950) and Kalinske (1947). The statistical characteristics of the entrainment, motions and deposition of bedload particles, and more specifically the probability density functions (p.d.f.s) of velocities, accelerations, travel times, hop distances and resting times are fundamental and of great importance to various applications in the fields of geology, hydraulics and environmental sciences (Chien & Wan 1999).

Laboratory experiments are direct and the most important means of collecting statistics for bedload particle motions. Different research groups around the world have performed high-resolution experiments over the past decades. Important results were obtained under different flow and sediment transport conditions. Regarding the p.d.f. of the streamwise velocities of bedload particles, for example, the exponential-like distributions were observed under subcritical flow conditions (Froude number $Fr < 1$) (Lajeunesse, Malverti & Charru 2010; Roseberry, Schmeeckle & Furbish 2012; Fathel, Furbish & Schmeeckle 2015; Liu, Pelosi & Guala 2019), while the Gaussian-like distributions were reported for supercritical flow conditions ($Fr > 1$) (Martin, Jerolmack & Schumer 2012; Ancey & Heyman 2014; Heyman, Bohorquez & Ancey 2016). This difference in the literature for the form of the velocity distribution was further investigated and explained by the two-regime scaling of the hop distance–time relation (Wu, Furbish & Foufoula-Georgiou 2020), which corresponds to two groups of particle hops (i.e. short and long trajectories) with distinct motion statistics. It is the mix of the two that leads to the exponential-like distribution, while the long hops alone result in the Gaussian-like distribution. Thus, the ratio of the two groups of hops, as closely related to the transport conditions, determines the specific form of the velocity distribution.

Regarding theoretical investigations for the kinematics of bedload particles based on these detailed experimental measurements, great progress has been made with the introduction and application of the Fokker–Planck (FP) equation for particle velocities. A general form of the FP equation, where the drift and diffusivity depend on the particle velocity, was introduced by Furbish, Roseberry & Schmeeckle (2012*b*) with reference to results in statistical mechanics. The form of the drift and diffusivity can be determined by calculating the first- and second-order moments of particle accelerations, respectively, according to measured trajectories of bedload particles. With specific assumptions involved, e.g. using the mean-reverting (or the Ornstein–Uhlenbeck) process to describe the stochastic velocity of a bedload particle during motions, a simpler form of the FP equation with a constant diffusivity can be obtained, which can be analytically solved under the equilibrium transport condition to give a truncated Gaussian distribution for the particle velocities (Ancey & Heyman 2014; Pierce, Hassan & Ferreira 2022). The exponential-like distribution for particle velocities can also be theoretically obtained by considering a different form of the FP equation with a constant diffusivity (e.g. Fan *et al.* 2014).

Following the previous work of Furbish *et al.* (2012*b*), Wu *et al.* (2020) revised the calculation of the acceleration by associating it with the linear interpolation for an

intermediate velocity (or the average velocity) as the starting point during analysing the same dataset used by Fathel *et al.* (2015). The most important results of the new analysis were the determination of the zero drift and the diffusivity depending exponentially on the particle velocity for the general form of the FP equation, correcting previous assessments in the literature (Furbish *et al.* 2012*b*). The corresponding Monte Carlo particle-tracking (individual-based) simulation was shown able to reproduce well the key features of the measured kinematic quantities for bedload particle hops, including that of velocities, accelerations, travel times, hop distances, as well as the identified two-regime scaling for the hop distance–time relation. Note that the form of the FP equation with the diffusivity depending exponentially on the velocity is not unique to bedload transport. It has also been discussed for other physical processes (Cherstvy & Metzler 2013; Wang *et al.* 2020), such as bombardment-enhanced diffusion (Maby 1976) and irradiation-enhanced diffusion (Kowall, Peak & Corbett 1976).

It is the lack of an analytical analysis for the continuum FP equation (due to difficulties in treating the velocity-dependent diffusivity) that has driven the application of the individual-based simulation to obtain numerical solutions. Aiming at conducting theoretical analysis enabling further exploration and discussions on the two-regime scaling relation, in a recent work, Wu *et al.* (2021) devised a velocity transformation mapping the physical velocity into an opportunely distorted velocity axis, resulting in a governing equation intrinsically identical to that of Taylor dispersion (Taylor 1953) for solute transport within shear flows. The major difference of this approach (Wu *et al.* 2021) from the earlier work (Wu *et al.* 2020) is the fundamental assumption of a prescribed pattern for the particle velocity variations. That is, it assumes that the particle is performing a Brownian motion in the stretched velocity dimension, which can be compared with the work of Ancey & Heyman (2014) prescribing a mean-reverting process for the particle velocity. Instead, the governing equation used by Wu *et al.* (2020) was determined from the general form of the FP equation (Furbish *et al.* 2012*b*) by experimentally obtaining the drift and diffusivity terms according to their definitions. Consequently, although the obtained theoretical expression (Wu *et al.* 2021) captures perfectly the measured data, the relationship between corresponding drift and diffusivity in the governing equation was shown to follow a certain fixed form, which may or may not be the case for the bedload particle transport. Thus, there is still a need to find an analytical method to treat the exponentially velocity-dependent diffusivity for the FP equation as introduced and discussed by Furbish *et al.* (2012*b*) and Wu *et al.* (2020).

One more obstacle for analytically solving the FP equation lies in specifying an appropriate (velocity) boundary condition for particles ceasing their motions. This condition may be straightforward if observing the particle hop from the Lagrangian perspective: the particle may stop its motion when its velocity decreases to zero, as specified in previous simulations (Furbish *et al.* 2012*b*; Fan *et al.* 2014, 2016). And it is also straightforward if we assign a stopping chance for the particle at each time when its velocity drops to (or below) zero, as a means of generally describing how easily the particle can stop its motion, the value of which of course is related to the transport environment. In the individual-based numerical simulation by Wu *et al.* (2020), a stopping chance of 10 % was determined by comparing the mean travel time of the simulation with that of the measured data. It remains unknown how to translate such a motion termination condition (from the Lagrangian perspective) into the boundary condition for the governing FP equation (from the Eulerian perspective), and whether there is a means of directly estimating the corresponding parameter based on the measurements.

This work is to provide a full analytical consideration for the particle hop process as simulated by Wu *et al.* (2020), by tackling the above-mentioned two unsolved problems.

First, we propose a deposition boundary condition for the FP equation accounting for the cease of motions of particles as physically required by the hop process. It is actually a simple Robin (the third-type) boundary condition, with an important parameter representing the deposition rate of bedload transport. Secondly, for the analytical solutions of hop statistics, a new variable transformation is devised to treat the exponentially velocity-dependent diffusivity. The original bedload transport problem can be transformed into a classic problem of solute transport in shear flows through a tube with a constant diffusivity. We have also obtained analytical expressions relating our newly introduced physical parameter of the deposition rate to the mean travel time and the mean hop distance, which is another important contribution of this work. We emphasize that we can now directly determine the deposition rate based on the measured particle motion statistics, instead of resorting to a fitting procedure matching the predicted quantities to the measurements, as done in the numerical simulation of the previous study (Wu *et al.* 2020).

The rest of this paper is structured as follows. For the bedload transport problem formulated in § 2 using an FP equation based on the experiment of Roseberry *et al.* (2012), we first specify its initial condition and the deposition boundary condition. Then, we show how to use spatial and temporal moments to express the key statistics of the hop events, including the distributions of travel times and hop distances, and the mean hop distance over travel time. To find their analytical solutions, a new variable transformation is provided in § 3, greatly simplifying the transport problem. After verifying the analytical result with the numerical and experimental results, we further investigate the influence of the deposition condition on these three key characteristics in § 4. Analytical expressions are obtained relating the deposition rate to the mean travel time, and the mean hop distance. In § 5, we further explore the variation of the deposition rate under different flow conditions, using the recent experimental data of Liu *et al.* (2019). Finally, § 6 concludes.

2. Formulations

2.1. *Governing equation*

We consider the bedload transport under subcritical flow conditions (with Froude number $Fr < 1$), which is in accordance with that analysed by Fathel *et al.* (2015) and Wu *et al.* (2020). Six runs of experiments (R1A, R2A, R3A, R5A, R2B and R3B) were conducted by Roseberry *et al.* (2012) using relatively uniform sand ($D_{50} = 0.05$ cm) in an 8.5m $\times$ 0.3m flume under four different flow conditions. The flow rate was low and thus no bed form was produced. The run R3B was later reanalysed by Fathel *et al.* (2015) and it is the main dataset used in the current analysis. Some key experimental parameters are listed in table 1. More details can be found in the work of Roseberry *et al.* (2012).

We aim at studying particle hops which are defined as trajectories of particles moving successively from the start to the end of their motions, as shown in figure 1. For simplicity, only the streamwise motions of bedload particles are considered, enabling an idealized theoretical analysis. Statistics of particle motions including velocities, accelerations, travel times and hop distances can all be obtained based on tracing the particle's streamwise positions x^* and recording the corresponding times t^*.

For the individual-based simulation by Wu *et al.* (2020), the stochastic differential equation (SDE) can be written as

$$\frac{\mathrm{d}x^*}{\mathrm{d}t^*} = u^*, \tag{2.1a}$$

Description	Parameter	Reference value
Depth of water	H^*	12.5 cm
Velocity at 1 cm	U_1^*	31.0 cm
Median sediment particle size	D_{50}	0.05 cm
Run time	T_{run}^*	0.4 s
Sampling interval	Δt^*	0.004 s
Froude number	Fr	0.30–0.35
Shields number	θ	0.05
Particle Reynolds number	Re_p	22.76
Average hop distance	L_a^*	0.46 cm
Average travel time	T_a^*	0.97 s
Average particle velocity	u_a^*	4.76 cm s^{-1}
Coefficient for velocity diffusivity	k_0^*	300 cm^2 s^{-3}
Reference velocity for diffusivity	u_0^*	4.76 cm^2 s^{-1}
Deposition rate	Γ_s^*	48.8 cm^2 s^{-2}
Time step for simulations	Δt_s^*	0.0004 s

Table 1. Parameters and hop statistics of the experiments by Roseberry *et al.* (2012) (reanalysed by Fathel *et al.* 2015) and the simulation by Wu *et al.* (2020).

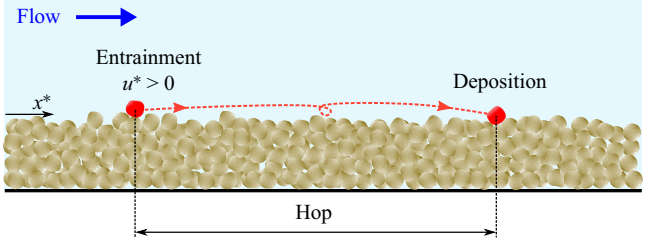

Figure 1. Sketch of a bedload particle hop.

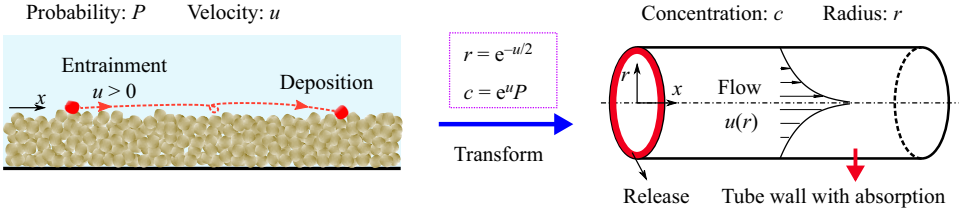

Figure 2. Schematic representation of the transformation (3.3*a*,*b*).

$$\frac{\mathrm{d}u^*}{\mathrm{d}t^*} = a_\mu^*(u^*) + \sqrt{2k^*(u^*)}\xi^*(t^*), \tag{2.1b}$$

where x^* is the streamwise location, t^* is the time, u^* is the streamwise velocity, a_μ^* is the 'drift' term of velocity, k^* is the diffusion coefficient of velocity and ξ^* is the white noise term. We use the asterisk to mark dimensional variables (which will be non-dimensionalized later in § 3.1).

According to the reanalysis (Wu *et al.* 2020, figure 1) of the experimental data as presented by Fathel *et al.* (2015), the drift term is zero, and the diffusivity k^* is an exponential function of u^* due to the observed exponential distribution of particle

velocities (Wu *et al.* 2020, (6)), namely

$$a_\mu^* = 0, \quad k^*(u^*) = k_0^* \, \mathrm{e}^{u^*/u_0^*}. \tag{2.2a,b}$$

The reference velocity u_0^* is in fact equal to the mean velocity u_a^*; and in the simulation of Wu *et al.* (2020), $u_0^* = u_a^* = 4.76\ \mathrm{cm\ s^{-1}}$ and the constant $k_0^* = 300\ \mathrm{cm^2\ s^{-3}}$. Technically, this velocity dependence of the diffusivity k^* becomes the main obstacle for analytically analysing the corresponding FP equation.

Note that (2.2*a*,*b*) represents one of the limited sets of drift and diffusivity that has been directly determined based on available experimental dataset of particle kinematics under subcritical flow conditions (Roseberry *et al.* 2012; Liu *et al.* 2019). It represents the external force (as a result of the combined actions of turbulent flow drag, particle–particle and particle–bed interactions) acting on the moving bedload particles, and states the nature of its random variations. The model (2.1) describes a Markov process and thus it cannot account for the historical effect of the velocity variations. There are other forms of the drift $a_\mu^*(u^*)$ and the diffusivity $k^*(u^*)$ depending on the flow and transport conditions, as discussed in §§ 1 and 6.

For the continuum model, we can deduce the FP equation immediately from (2.1), which is similar to (3.9) of Ancey & Heyman (2014). We use $P^*(x^*, u^*, t^*)$ to denote the joint p.d.f. of the streamwise position, the velocity and the time; then the governing equation can be written as

$$\frac{\partial P^*}{\partial t^*} + u^* \frac{\partial P^*}{\partial x^*} = \frac{\partial^2}{\partial u^{*2}} (k_0^* \, \mathrm{e}^{u^*/u_0^*} P^*), \tag{2.3}$$

with $u^* \in (0, \infty)$ and $x^* \in (-\infty, \infty)$.

2.2. *Initial and boundary conditions*

Since we are focusing on the particle hop process, we need to describe the start of the particle motion (entrainment), the successive streamwise movement of the particle and, eventually, the cease of motion of this particle (deposition). While the successive particle motions are governed by (2.3), the entrainment and deposition phases of the hop process are specified by the initial and boundary conditions for (2.3), respectively.

First, for the entrainment of bedload particles, we follow Wu *et al.* (2021) and consider all bedload particles initially starting their motions at $x^* = 0$ with $u^* = 0$. Thus, the initial condition is

$$P_{init}^* = \delta(x^*)\delta(u^*), \tag{2.4}$$

where δ is the delta function. Note that (2.4) is a rather idealized description for the entrainment. During analysis of the particle hop statistics (e.g. velocities, accelerations, travel times and hop distances), an important but straightforward simplification is that all the information will not depend on when and where the particle hop starts. Hence, by introducing (2.4) we virtually move all the starting positions to the same location for the ensemble of hops and start their motions at the same time.

Second, we can specify the deposition boundary condition according to the numerical algorithm of Wu *et al.* (2020). We assume that a particle may cease its motion with a stopping chance P_{stop} every time its velocity drops to (or below) zero. Wu *et al.* (2020) chose a value of $P_{stop} = 10\,\%$ so that the mean travel time of the simulated particle hops can match that of the experimental measurements (Fathel *et al.* 2015). Therefore, we can

impose

$$k_0^* \frac{\partial P^*}{\partial u^*}\bigg|_{u^*=0} = \Gamma^* P^*|_{u^*=0}, \tag{2.5}$$

where the deposition rate Γ^* can be related to P_{stop}. Equation (2.5) is a Robin (third-type) boundary condition for partially reflecting boundaries, often used in reactive transport problems (Singer *et al.* 2008; Andrews 2009; Jiang *et al.* 2022; Wang *et al.* 2022*b*). According to the relationship between the individual-based and continuum models, P_{stop} used in the simulation can be calculated (Erban & Chapman 2007, (10)) as

$$P_{stop} = \Gamma^* \sqrt{\frac{\pi \Delta t_s^*}{k_0^*}}, \tag{2.6}$$

where Δt_s^* is the time step and $\Delta t_s^* = 0.0004$ s was used in the simulation of Wu *et al.* (2020). Therefore, Γ^* can be obtained by (2.6) as

$$\Gamma^* = \Gamma_s^* = 48.8 \text{ cm s}^{-2}. \tag{2.7}$$

Generally speaking, Γ^* determines how easily a particle will cease its motion. Its value may be related to the roughness of the bed, the flow strength, fluid–particle interactions, particle–bed collisions, the particle diameter, etc. As discussed by Wu *et al.* (2020), bedload particles moving at low speeds may encounter the zero velocity situation (or 'zero velocity hits') many times and thus stop early, resulting in short hop distances. Particles performing long hops are probably spending more time moving with velocities much greater than zero and thus have fewer chances to encounter the zero velocity hits. One extreme case is that bedload particles cease their motions immediately when $u^* = 0$, as in the condition imposed in the random walk simulations by Furbish *et al.* (2012*b*) and Fan *et al.* (2016). It is mathematically similar to an absorbing boundary with $\Gamma^* \to \infty$.

Note that Γ^* is more physically meaningful than P_{stop} because the value of P_{stop} varies with the time step chosen for simulations. On the other hand, another contribution of this work, as documented in § 4.2.2, is that we have analytically related this new physical parameter of the deposition rate Γ^* to the mean travel time and the mean particle velocity, for example. Consequently, Γ^* can be directly determined based on the measured particle hop statistics, in contrast to the previous work of Wu *et al.* (2020) in which a similar parameter to P_{stop} needs to be obtained by fitting the predicted quantities to experimental measurements.

2.3. *Travel times and hop distances: relation to moments*

Now we have the continuum model based on exploring the individual-based simulation algorithm of Wu *et al.* (2020), we can express the key statistics of hop events of bedload particles, such as the distributions of travel times and hop distances, using the spatial and temporal moments of P^*.

First, we derive the p.d.f. of travel times $f_T^*(t^*)$, which is the period of time of a hop. By the deposition condition (2.5), the probability flux of stopped particles (from the motion

state to the resting state) is $\Gamma^* P^*(x^*, u^* = 0, t^*)$. Therefore

$$f_T^*(t^*) = \int_{-\infty}^{\infty} \Gamma^* P^*(x^*, u^* = 0, t^*)\,\mathrm{d}x^* = \Gamma^* \mu_0^*(u^* = 0, t^*), \tag{2.8}$$

where μ_0^* is the zeroth-order spatial moment and its definition extended to the nth-order spatial moment is

$$\mu_n^* \triangleq \int_{-\infty}^{\infty} (x^*)^n P^*\,\mathrm{d}x^*, \quad n = 0, 1, \ldots. \tag{2.9}$$

Additionally, note that the total number of particles (both in motion and at rest) is conserved, thus f_T^* can also be expressed as

$$f_T^* = \frac{\mathrm{d}}{\mathrm{d}t^*}(1 - \overline{\mu_0^*}) = -\frac{\mathrm{d}\overline{\mu_0^*}}{\mathrm{d}t^*}, \tag{2.10}$$

where we use the bar to denote the mean of a value over u^*, namely

$$\overline{\mu_0^*} = \int_0^{\infty} \mu_0^*\,\mathrm{d}u^*. \tag{2.11}$$

Second, we can use the temporal moment of P^* to express the p.d.f. of hop distances

$$f_L^*(x^*) = \int_0^{\infty} \Gamma^* P^*(x^*, u^* = 0, t^*)\,\mathrm{d}t^* = \Gamma^* m_0^*(x^*, u^* = 0), \tag{2.12}$$

where m_0^* is the zeroth-order temporal moment (Harvey & Gorelick 1995) and

$$m_n^* \triangleq \int_0^{\infty} (t^*)^n P^*\,\mathrm{d}t^*, \quad n = 0, 1, \ldots. \tag{2.13}$$

Finally, we analyse the mean hop distance over travel time, namely the mean of all possible hop distances at each specific travel time. Thus, the mean hop distance is a function of travel time, denoted as $L^*(t^*)$. It can be calculated using the first two spatial moments of the stopped particles

$$L^*(t^*) = \frac{\displaystyle\int_{-\infty}^{\infty} x^* \Gamma^* P^*|_{u^*=0}\,\mathrm{d}x^*}{\displaystyle\int_{-\infty}^{\infty} \Gamma^* P^*|_{u^*=0}\,\mathrm{d}x^*} = \frac{\mu_1^*|_{u^*=0}}{\mu_0^*|_{u^*=0}}. \tag{2.14}$$

By (2.14), we can see a different physical meaning of $L^*(t^*)$: the position of the centroid of the particle cloud stopped at a specific time t^*; because μ_1^*/μ_0^* is actually the normalized first-order moment.

3. Analytical solutions for hop statistics

Based on the continuum model we have revealed the relationship between the key hop statistics and moments. Next, we will analytically solve the three key characteristics, i.e. the p.d.f.s of travel times ($f_T^*(t^*)$) and hop distances ($f_L^*(x^*)$), and the mean hop distance over travel time ($L^*(t^*)$).

As mentioned previously, the major obstacle for us to analytically treat (2.3) is the exponentially velocity-dependent diffusivity ($k^*(u^*)$). To tackle this difficulty we devise

a variable transformation, based on which (2.3) can be transformed into a much simpler form, representing the main contribution of this work. Then we can directly apply the method of Barton (1983) to obtain the analytical expressions of spatial and temporal moments, and thus obtain f_T^*, f_L and L^*.

3.1. *Non-dimensionalization and the variable transformation*

Before introducing the transformation for the velocity-dependent $k^*(u^*)$, we non-dimensionalize the governing equation (2.3) with the following dimensionless variables and parameters:

$$\left.\begin{aligned} u = \frac{u^*}{u_0^*}, \quad x = \frac{x^*}{4(u_0^*)^3/k_0^*}, \quad t = \frac{t^*}{4(u_0^*)^2/k_0^*}, \\ \Gamma = \frac{2\Gamma^*}{k_0^*/u_0^*}, \quad k = \frac{k^*}{k_0^*} = \mathrm{e}^u, \quad P = \frac{4P^*}{k_0^*/(u_0^*)^4}, \end{aligned}\right\} \tag{3.1}$$

where constants 4 and 2 are imposed for the subsequent transformation. The resulting dimensionless governing equation and boundary condition are

$$\frac{\partial P}{\partial t} + u\frac{\partial P}{\partial x} = 4\frac{\partial^2}{\partial u^2}(\mathrm{e}^u P), \quad u \in (0, \infty),\ x \in (-\infty, \infty), \tag{3.2a}$$

$$\left.\frac{\partial(\mathrm{e}^u P)}{\partial u}\right|_{u=0} = \frac{\Gamma}{2} P|_{u=0}. \tag{3.2b}$$

Next, subject to *a posteriori* verification, we introduce the following transformation:

$$r = \mathrm{e}^{-u/2}, \quad c = \mathrm{e}^u P. \tag{3.3a,b}$$

Consequently, $u = -2\ln r$ and $P = c/k = r^2 c$. With the chain rule $\partial/\partial u = (\partial/\partial r)(\partial r/\partial u) = -\frac{1}{2} r(\partial/\partial r)$, the whole initial-boundary-value problem (2.3)–(2.4) can be rewritten as

$$\frac{\partial c}{\partial t} + u(r)\frac{\partial c}{\partial x} = \frac{1}{r}\frac{\partial}{\partial r}\left(r\frac{\partial c}{\partial r}\right), \quad r \in (0, 1),\ x \in (-\infty, \infty), \tag{3.4a}$$

$$\left.\frac{\partial c}{\partial r}\right|_{r=1} = -\Gamma c|_{r=1}, \tag{3.4b}$$

$$c|_{t=0} = \frac{1}{2}\delta(x)\delta(r-1). \tag{3.4c}$$

It is seen that the above transformation greatly simplifies the original FP equation (2.3) by transforming the problem of bedload transport with an exponentially velocity-dependent diffusivity into a classic problem of solute transport in laminar flows through a tube with a constant diffusivity. As a result, r is a 'radial' coordinate, which can be one-to-one mapped to the velocity u; c can be understood as the 'concentration' distribution; and the deposition boundary condition (2.5) at $u = 0$ becomes an absorption condition (3.4*b*) at the 'tube wall' ($r = 1$), the same as the classic reactive transport problems (Barton 1984; Wang & Chen 2017; Jiang & Chen 2018; Debnath *et al.* 2022). The transformation of u is different from the (2.19) of Wu *et al.* (2021) because, in their governing equation, the form of drift and diffusivity is fixed and implies a non-zero drift. Additionally, the form of r is similar to (25) of Cherstvy & Metzler (2013), which

is deduced from SDEs in the Stratonovich convention and thus requires an additional transformation back into equations in the Itô convention.

In addition, the integration of the p.d.f. can be written as

$$\int_{-\infty}^{\infty}\int_{0}^{\infty} P(x,u,t)\,\mathrm{d}u\,\mathrm{d}x = \int_{-\infty}^{\infty}\int_{0}^{1} 2rc(x,r,t)\,\mathrm{d}r\,\mathrm{d}x, \tag{3.5}$$

with the mean operation over the velocity u (2.11) rewritten in terms of r as

$$\bar{c} = \int_{0}^{1} 2rc\,\mathrm{d}r, \tag{3.6}$$

which is exactly the area-average operation over a tube cross-section.

Finally, we non-dimensionalize $f_T^*(t^*)$, $f_L^*(x^*)$ and $L^*(t^*)$ using (3.1) and (3.3*a*,*b*). Results of (2.8), (2.12) and (2.14) can be rewritten as

$$f_T(t) = 2\Gamma\mu_0(r=1,t), \tag{3.7}$$

$$f_L(x) = 2\Gamma m_0(x,r=1), \tag{3.8}$$

$$L(t) = \frac{\mu_1(r=1,t)}{\mu_0(r=1,t)}, \tag{3.9}$$

where the dimensionless spatial moment μ_n and temporal moment m_n are

$$\mu_n(r,t) \triangleq \int_{-\infty}^{\infty} x^n c(x,r,t)\,\mathrm{d}x, \quad m_n(x,r) \triangleq \int_{0}^{\infty} t^n c(x,r,t)\,\mathrm{d}t, \tag{3.10a,b}$$

respectively, and $n = 0, 1, 2, \ldots$.

3.2. *Solutions for spatial and temporal moments*

We can solve the spatial moment μ_n for f_T and L in (3.7) and (3.9). Note that the transport problem (3.4) is only slightly different from the classic Taylor dispersion of solute in a tube flow (Taylor 1953; Aris 1956): the 'velocity distribution' is $u(r) = -2\ln r$ instead of the parabolic profile, and there is no longitudinal diffusion.

The solutions of spatial moments have been systematically studied by Barton (1983, 1984) using the Sturm–Liouville theory, with general expressions for the first four moments provided for direct use. Barton's results have been widely applied to studies on various dispersion phenomena (Zeng *et al.* 2011; Li *et al.* 2018; Guan *et al.* 2022; Wang, Jiang & Chen 2022*a*). In order not to disrupt the narrative flow, the solution procedure is summarized in Appendix A of § A.1.

For f_L in (3.8), we can solve the temporal moment μ_0. The solution procedure is similar to that of the spatial moments as presented above, and details are given in Appendix A of § A.2. Since there is no longitudinal diffusion in the transport problem (3.4), x can be seen as a 'time' variable in the resulting moment equations. Consequently, the form of the solution of μ_0 is the same as (A5): one only needs to replace t using x with corresponding eigenvalues and eigenfunctions. The generalized integral transform technique (GITT) method (Cotta 1993) is applied to solve the corresponding eigenvalue problem.

4. Results

We have deduced the continuum model for the bedload particle hops. A simple deposition boundary condition for particles ceasing their motions was specified for the governing

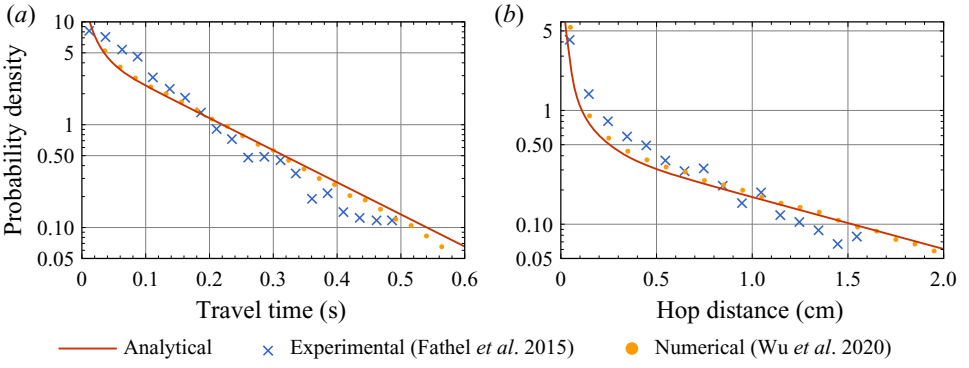

Figure 3. The p.d.f.s of (*a*) travel times f_T, and (*b*) hop distances f_L.

equation based on recent numerical and experimental studies. We then analytically solved the three key characteristics: the p.d.f.s of travel times ($f_T(t)$) and hop distances ($f_L(x)$), as well as the mean hop distance over travel time ($L(t)$). Here we continue to investigate the influence of the deposition condition on these key characteristics of hop events.

4.1. *Validation by experimental and numerical results*

We first validate our analytical results for the three key characteristics by the experimental data of Fathel *et al.* (2015) and the numerical simulations of Wu *et al.* (2020). Note that analytical expressions such as (A5) and (A8) contain series expansions which need to be truncated. We adopted the first ten eigenvalues and eigenfunctions for the analysis. Additionally, although we have non-dimensionalized the governing equation and thus corresponding analytical solutions, expressions with dimensional variables are also deduced, enabling a direct comparison with existing experimental and numerical results (e.g. Wu *et al.* 2020, figures 3 and 4).

4.1.1. *The p.d.f.s of travel times and hop distances*

As shown in figure 3(*a*), the analytical result for the p.d.f. of travel times agrees well with the numerical result, which is close to the experimental measurements. For large travel times, f_T decays exponentially with a rate almost equal to the first non-zero eigenvalue, as shown by (3.7) and (A5). For small travel times, we can observe a noticeable deviation of the numerical and analytical results from the experimental data, where the measurements roughly follow an exponential decay, while the other two results decrease more sharply. The reason for this discrepancy may be twofold. On the one hand, there exist difficulties in experimentally tracking very short hops, giving rise to uncertainties for the corresponding measurements. On the other hand, it may also be related to the deposition boundary condition which may not exactly agree with the physical process of how the particle ceases its motion. Mathematically, f_T approaches infinity as t approaches zero because the initial condition (2.4) is a delta function of u^* at $u^* = 0$.

Comparisons for p.d.f.s of hop distances among different results also demonstrate good consistency, as shown in figure 3(*b*). Similar to the travel time distribution, for large hop distances f_L decays exponentially, as revealed by (3.8) and (A14). For small hop distances, f_L decreases sharply and thus is closer to a Weibull distribution (Fathel *et al.* 2015). Namely, f_L has a Weibull front and an exponential tail, as pointed out by Wu *et al.* (2020) and Wu *et al.* (2021).

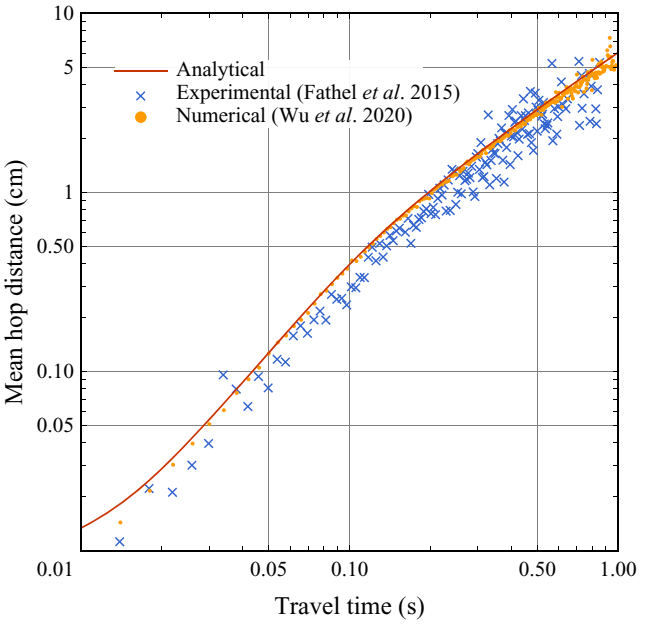

Figure 4. Mean hop distance over travel time $L(t)$.

4.1.2. *Mean hop distance over travel time*

For the mean hop distance over travel time $L(t)$, comparisons in figure 4 show an overall similar feature among analytical, numerical and experimental results. That is, very good agreement between the first two results in fact demonstrates the validation of the analytical solution, since the two approaches consider almost the same idealized transport process; their deviations from the experimental measurements highlight the limitation possibly related to the deposition boundary condition, or the uncertainties of the measurements. Specifically, the two-regime scaling relation (advective $L \sim t^2$ and dispersive $L \sim t$) is consistent with previous analysis (Wu *et al.* 2020, 2021). The deviation of the analytical solution at very short travel times (here $t^* < 0.02$s) may be due to the Gibbs phenomenon of series expansion because the initial condition (2.4) is a delta function of u^* at $u^* = 0$, based on which the mean hop distance over travel time in (2.14) is calculated.

4.2. *Influence of deposition rate*

The key parameter introduced in this work is the deposition rate Γ^*. In the calculation in § 4.1, $\Gamma_s^* = 48.8\ \mathrm{cms}^{-2}$ in (2.7) is used based on the experimental and numerical studies (Wu *et al.* 2020). Here, we analyse the effect of Γ^* on the particle hop statistics, which may correspond to the influence of different transport conditions including the flow strength, the roughness of the bed and the slope of the bed. Two additional cases with $\Gamma^* = 0.2\Gamma_s^*$ and $\Gamma^* = 5\Gamma_s^*$ are considered, while other parameters are kept the same, for the three key characteristics: $f_T(t)$, $f_L(x)$ and $L(t)$. Importantly, we eventually deduced the relation between the deposition rate and the average travel time, or between that and the average hop distance. This provides a means to directly determine the deposition rate based on the physically measured particle motion statistics, instead of fitting the predicted results to the measurements.

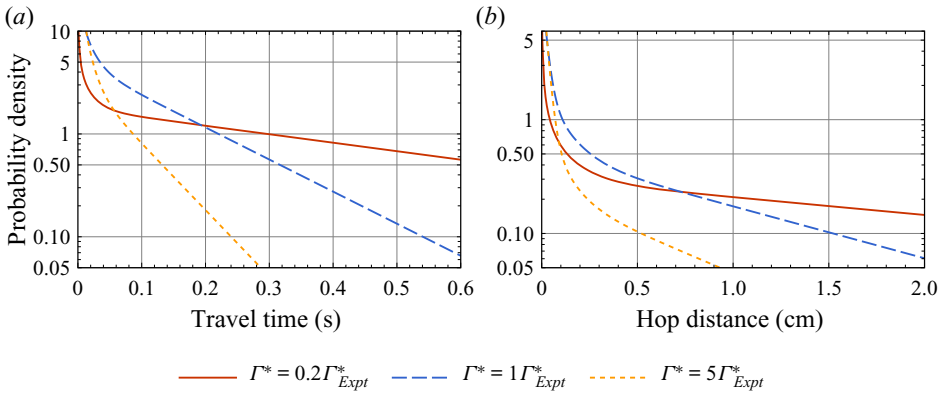

Figure 5. The p.d.f.s of (*a*) travel times and (*b*) hop distances for different deposition rates.

4.2.1. *The p.d.f.s of travel times and hop distances*

The influence of Γ^* on the p.d.f. of travel times is shown in figure 5(*a*). It is seen that the larger the Γ^* is, the smaller the proportion of long travel times is, and the larger the proportion of short travel times is. This can be observed partly by the different slopes of the exponential tail of the three curves. Since Γ^* is proportional to the stopping chance as shown in (2.6), a larger Γ^* means that particles are more likely to stop when its velocity decreases to zero, on average resulting in smaller travel times. For the hop distance, similarly, increasing the deposition rate can generally reduce the hop length; and the resulting change in shape for curves of f_L is analogous to that for f_T, as shown in figure 5(*b*).

4.2.2. *Relation of deposition rate to the average travel time and average hop distance*

Other than revealing the effect of deposition rate on the shape of the p.d.f.s of travel times and hop distances, it is interesting to observe how the mean travel time and hop distance will depend on the deposition rate.

In figure 6, we have calculated and displayed T_a and L_a as functions of the deposition rate. Interestingly, a rather good power-law relation can be observed for both mean quantities, which motivates us to see whether some theoretical description would be possible. We have eventually arrived at analytical expressions of T_a and L_a in terms of Γ, enabling a direct determination of this new quantity Γ based on measured particle statistics, instead of the fitting process used for the similar parameter of particle stopping chance in the numerical simulation of the previous study (Wu *et al.* 2020). Here, we document the deduction of this key result.

Mathematically, the mean travel time T_a and hop distance L_a are the first-order moments of the p.d.f.s of travel times and hop distances, respectively. With the aid of (3.7) and (3.8),

$$T_a \triangleq \int_0^\infty t f_T(t)\,\mathrm{d}t = \int_0^\infty t 2\Gamma\mu_0(r=1,t)\,\mathrm{d}t = 2\Gamma M_{0,1}(r=1), \tag{4.1}$$

$$L_a \triangleq \int_{-\infty}^\infty x f_L(x)\,\mathrm{d}x = \int_{-\infty}^\infty x 2\Gamma m_0(x,r=1)\,\mathrm{d}x = 2\Gamma M_{1,0}(r=1), \tag{4.2}$$

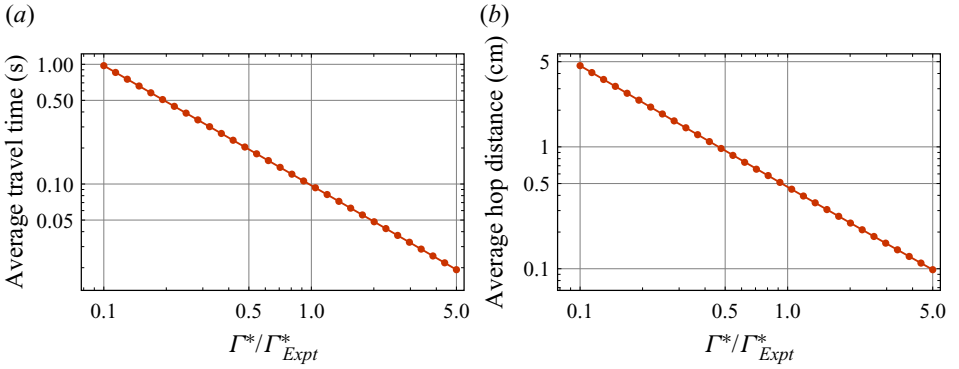

Figure 6. (*a*) Mean travel time T_a and (*b*) mean hop distance L_a, as functions of the deposition rate Γ.

where $M_{n,m}$ is introduced as the 'universal' moment, i.e. the temporal–spatial moment

$$M_{n,m} \triangleq \int_0^\infty t^m \int_{-\infty}^\infty x^n c(x, r, t)\,\mathrm{d}x\,\mathrm{d}t, \tag{4.3}$$

for $n = 0, 1, 2, \ldots$ and $m = 0, 1, 2, \ldots$.

Universal moments $M_{0,1}$ and $M_{1,0}$ can be solved, as presented in Appendix B. By (B4*a*,*b*), (B3) and (B7), we have

$$T_a = \bar{M}_{0,0} = \frac{1}{2\Gamma}, \tag{4.4}$$

$$L_a = 2\Gamma M_{1,0}|_{r=1} = \overline{-u(r)M_{0,0}} = \frac{1}{2\Gamma}. \tag{4.5}$$

Namely, the power-law relation as observed in figure 6 is in fact a reciprocal function of Γ.

Finally, we can express the results by the original dimensional variables in (3.1). Equations (4.4) and (4.5) turn out to be

$$T_a^* = \frac{u_0^*}{\Gamma^*} = \frac{u_a^*}{\Gamma^*}, \tag{4.6a}$$

$$L_a^* = \frac{(u_0^*)^2}{\Gamma^*} = u_0^* T_a^* = u_a^* T_a^*. \tag{4.6b}$$

Note that u_0^* is equal to the mean particle velocity u_a^*, and Γ^* has dimensions of acceleration. Additionally, considering the physical meaning of the deposition rate Γ^*, which describes how fast the particle stops its motions, another interpretation of (4.6) can be given as follows. The mean travel time is the time when a particle travelling with the mean velocity u_a^* decelerates until it is stopped under the acceleration Γ^*. The mean hop distance is simply the distance during the deceleration phase, $u_a^* T_a^*$. Note that the mean velocity u_a^* is the average of the measured velocities at each discrete point of the hop trajectories and thus, $u_a^* = L_a^*/T_a^*$. (4.6*b*) reveals no new findings.

In § 2.2, we have used P_{stop} in the individual-based simulation of Wu *et al.* (2020) to determine Γ^* by (2.6), and $\Gamma^* = 48.8$ cm s^{-2} was obtained. We need to emphasize that P_{stop} was fitted so that the simulated mean travel time can match the measured result.

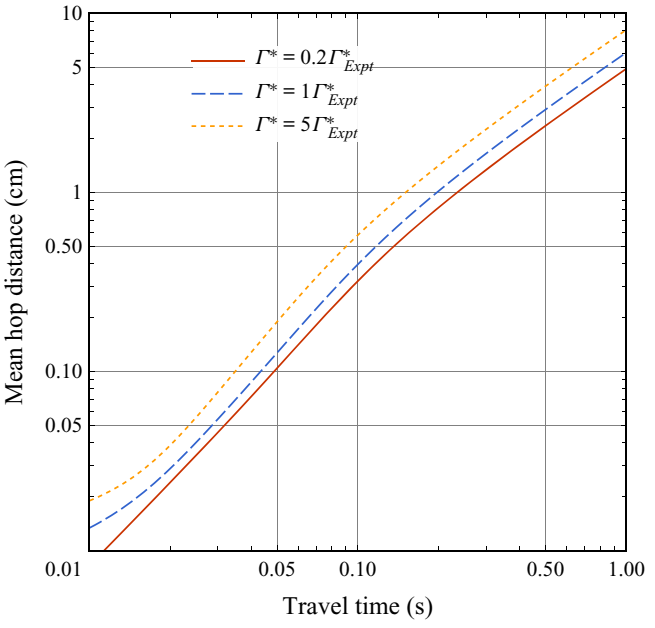

Figure 7. Mean hop distance over travel time $L(t)$ for different deposition rates.

Now, we can directly use the experimental data to calculate Γ^* based on (4.6)

$$\Gamma^* = \frac{u_a^*}{T_a^*} = \frac{(u_a^*)^2}{L_a^*} = \frac{L_a^*}{(T_a^*)^2}. \tag{4.7}$$

The mean travel time in figure 3(*a*) is 0.97 s (see table 1), which gives $\Gamma^* = 49.1$ cm s^{-2}, very close to the value used in the numerical simulation.

4.2.3. *Mean hop distance over travel time*

For the mean hop distance over travel time displayed in figure 7, the influence of the deposition rate may appear rather counter-intuitive at first glance: when Γ^* increases, $L(t)$ does not decrease as expected given particles would generally have shorter hop distances (as demonstrated in figure 5*b*); but instead $L(t)$ increases with Γ^*.

We recall the physical meaning of $L(t)$ by (2.14): it tells us, on average, how far the particle can travel during a hop with a specific travel time. What $L(t)$ does not tell us is the distribution of particles with respect to travel times: by curves in figure 7 alone we have no idea of the proportion of particles that can travel as long as, say, around $t_e = 0.5$ s. Thus, for a higher deposition rate there are indeed fewer particles that can travel the same period of time t_e.

On the other hand, the deposition boundary condition requires that particles are about to stop motions by experiencing on average the same number of times when their velocities drop to zero with a given deposition rate. This means that, at a higher deposition rate, particles travel a period of t_e not because they survived more 'zero velocity hits' (than at a lower deposition rate), but because they generally travelled with a higher velocity which reduces their chance of experiencing a 'zero velocity hit'. Hence, a higher mean velocity during the hop results in a longer hop distance with the same travel time.

Description	Parameter	Units	Experiment S2	S3	S4	S5
Depth of water	H^*	cm	16.9	17.2	17.7	17.9
Velocity at 1.5 cm	$U^*_{1.5}$	cm	34	35	37	38
Median sediment particle size	D_{50}	cm	0.11	—	—	—
Run time	T^*_{run}	s	20	—	—	—
Sampling interval	Δt^*	s	1/120	—	—	—
Cutoff velocity	u^*_c	cm s^{-1}	1.5	—	—	—
Froude number	Fr		0.279	0.280	0.294	0.300
Shields number	θ		0.029	0.032	0.035	0.042
Particle Reynolds number	Re_p		73.41	86.55	93.13	94.22
Average hop distance	L^*_a	cm	0.696	0.770	0.817	0.885
Average travel time	T^*_a	s	0.13	0.12	0.13	0.13
Average particle velocity	u^*_a	cm s^{-1}	6.7	7.9	8.5	8.6
Standard deviation of acceleration	a^*_{std}	cm s^{-2}	444	524	538	605
Coefficient for velocity diffusivity by (5.4)	k^*_0	cm^2 s^{-3}	109.28	165.57	173.07	225.73
Reference velocity for diffusivity by (5.1)	u^*_0	cm s^{-1}	3.85	4.92	4.78	5.31
Deposition rate by (5.3*b*)	Γ^*	cm s^{-2}	29.65	40.97	36.80	40.82
Deposition frequency by (5.5)	f^*_d	s^{-1}	5.45	7.47	5.72	5.57

Table 2. Parameters and hop statistics for the experiments by Liu *et al.* (2019) and for the current model; S2–S5 are labels of different experiment series. The hyphen (-) represents that this parameter is the same for all the series.

5. Application to recent experiments: additional validation

As shown in the above sections, this present model works well for the single dataset by Fathel *et al.* (2015). It is thus interesting to check its performance against bedload particle hops under different transport conditions, which can provide additional validation for the model in its ability to generally describe the kinematics of particle motions. To this end, we choose experiments conducted recently by a different research group of Liu *et al.* (2019), who used much coarser sediment particles ($D_{50} = 0.11$ cm) with much larger particle Reynolds numbers, representing distinct transport characteristics from that of Fathel *et al.* (2015).

The experiments of Liu *et al.* (2019) were conducted in a 19m $\times$ 0.9m flume under five low flow rates. They provided five series (S1–S5) of data, with the Froude number varying from 0.27 to 0.30. Main experimental parameters are provided in table 2 and details can be found in their paper. Hereinafter, we follow Liu *et al.* (2019) and focus on the experimental series S2–S5 in the analysis, because a very limited number of moving particles were detected in S1 under the lowest shear-stress condition.

For the particle velocities, Liu *et al.* (2019, (1)) reported a gamma distribution which is closely related to the algorithm for distinguishing between motion and rest regimes during bedload particle transport, as argued by the authors: 'if we consider all the non-zero particle velocities, including both the motion and the ambiguous rocking back-and-forth state, the velocity distributions maintain the *exponential trend* in a lower range'. On the other hand, we note that the current model (2.3) adopts an exponential distribution as an approximation for the observed exponential-like form of the particle velocity distribution, the form of which generally applies to the observations of Liu *et al.* (2019) for particle velocities, thus (2.3) is expected to be able to describe the hop processes for this new dataset.

5.1. *Determine model parameters by experimental statistics*

We can determine the model parameters (i.e. u_0^*, Γ^* and k_0^*) directly by the experimental statistics according to the obtained theoretical result of (4.7). One important issue that needs to be addressed is that Liu *et al.* (2019) have imposed a cutoff velocity ($u_c^* = 1.5$ cm s^{-1}) to determine the start and the end of a particle hop. Namely, particles with velocities smaller than u_c^* are considered to be in the resting state. As a result, the reference velocity u_0^* in the governing equation (2.3) may not be equal to the mean velocity u_a^*. This treatment may also be responsible for the observed deviation from the exponential distribution of particle velocities at small values, as discussed above. In fact, by (C6), we have $u_0^* = u_a^* - u_c^*$. According to the experimental dataset of Liu *et al.* (2019) (table 2), we found that the average velocity $u_a^* > L_a^*/T_a^*$, which means that the experimental hop statistics do not satisfy the relationship in (4.6*b*). This inconsistency may arise from the filter of particle velocities for small values during the data analysis (Liu *et al.* 2019, p. 2672). To resolve this problem, we adopt the result of (4.6*b*) rather than the 'filtered' value for u_a^*. Therefore, the reference velocity is calculated by

$$u_0^* = \frac{L_a^*}{T_a^*} - u_c^*. \tag{5.1}$$

Next, we need to calculate Γ^* in the deposition boundary condition (2.5), which is now changed to

$$k_0^* \, \mathrm{e}^{u_c^*/u_0^*} \left.\frac{\partial P^*}{\partial u^*}\right|_{u^*=u_c^*} = \Gamma^* P^*|_{u^*=u_c^*}, \tag{5.2}$$

due to the introduced cutoff velocity. Fortunately, we can make a velocity translation ($u'^* = u^* - u_c^*$) to handle this issue, so that the corresponding analytical procedure remains nearly the same as before. Details of the derivation are presented in Appendix C. Note that by (C7), the relationship in (4.7) is now generalized as

$$\Gamma^* = \frac{u_a^* - u_c^*}{T_a^*} = u_a^* \frac{u_a^* - u_c^*}{L_a^*} \tag{5.3a}$$

$$= \frac{L_a^*}{(T_a^*)^2} - \frac{u_c^*}{T_a^*}, \tag{5.3b}$$

after the introduction of the cutoff velocity. We eventually calculated Γ^* based on (5.3*b*).

For the velocity diffusive coefficient k_0^*, we can use the experimental statistics of the acceleration distribution. Note that the acceleration distribution depends on the time step Δt^* used for measurements or numerical simulations. In the experiments of Liu *et al.* (2019), the time step $\Delta t^* = 1/120$ is small enough and we can use the Euler–Maruyama scheme to approximate the acceleration distribution, as presented in Appendix D. By (D17), k_0^* can be approximated by

$$k_0^* = \frac{\pi}{32} \Delta t^* (a_{std}^*)^2 \, \mathrm{e}^{-u_c^*/u_0^*}. \tag{5.4}$$

5.2. *Comparison of results under different flow rates*

With all model parameters determined (see table 2), we can obtain the analytical expressions for the three key characteristics and compare them with the experimental results of Liu *et al.* (2019). We also adopted the first ten eigenvalues and eigenfunctions for the analysis, the same as that in § 4.1.

Comparisons for the p.d.f.s of the travel times and hop distances for the four different flow rates are shown in figure 8. Although the analytical results can largely capture the shapes of the experimentally determined p.d.f.s, there are observable discrepancies especially for small travel times and short hop distances. The fact that the number of measured short hop events is much smaller than the expected value is probably due to the same reason as discussed in § 4.1.1. Apart from the 'unavoidable uncertainties in the automated particle-tracking process' as mentioned by Liu *et al.* (2019), another possible reason is that Liu *et al.* (2019) 'further and significantly restricted the whole datasets to long particle trajectories, with integrated displacement over $10D_{50}$, and experiencing at least one step-stop-step sequence of motion and rest'. Consequently, a large number of short trajectories were expected to be filtered during the data analysis, resulting in an underestimate of the proportion for short hop distances with small travel times.

For the mean hop distance over travel time $L(t)$, the analytical results show good agreement with the experimental results for all the four different flow rates, as shown in figure 9. Although the analytical result overestimated the portion of p.d.f.s for small travel times and short distances in figure 8, this theoretical model captures well the result of the mean hop distances during travel times spanning over two orders of magnitude, which is calculated for each travel time interval by dividing the measurements into bins. Since these bin statistics do not reflect the proportion (or relative magnitude) of hops travelling with different time periods, the result of the mean hop distance in figure 9 shows that the analytical model can correctly predict the information of, on average, how long a distance a particle can travel during the hop with a specific travel time.

The influence of flow condition on the p.d.f. of travel times and hop distances has been discussed by Liu *et al.* (2019). Here, we focus on its effect on the deposition rate. We have estimated Γ^* by (5.3*b*) using T_a^* and L_a^*. Table 2 and figure 8 show that the travel time distribution is insensitive to the flow rate, as reported by Liu *et al.* (2019), while the average hop distance increases with the flow rate. Therefore, informed by (5.3*b*), we know that the deposition rate may also grow as the flow rate increases, although the value of Γ^* for experiment S2 is larger than that of S3 because $T_a^* = 0.12$ s of S2 is the smallest. This overall increasing tendency of Γ^* over the flow rate for S3–S5 is rather counter-intuitive because it is expected that the deposition effect should be weakened as the bed shear stress increases. This can be explained by the fact that the velocity diffusion coefficient also increases with the flow rate. Therefore, to quantify the net effect of deposition, we introduce a new parameter according to the stopping probability in (2.6)

$$f_d^* \triangleq \frac{(\Gamma^*)^2}{k_0'^*} = \frac{(\Gamma^*)^2}{k_0^* \, \mathrm{e}^{u_c^*/u_0^*}}, \tag{5.5}$$

based on the deposition boundary condition (5.2). The unit of f_d^* is s^{-1} and thus we call f_d^* the deposition frequency, which can reflect the stopping possibility of the deposition event. As a result, as shown in table 2, f_d^* decreases as the flow rate increases as expected for S3–S5. However, due to a lack of systematic experimental studies, at this stage, we cannot draw any further conclusions on the relation between the deposition frequency and the flow rate.

6. Concluding remarks

For the statistics of bedload particle hops in subcritical flows, this work has provided a full analytical consideration of the numerical simulations of Wu *et al.* (2020) based on the experimental data of Fathel *et al.* (2015), and the obtained analytical solutions are further

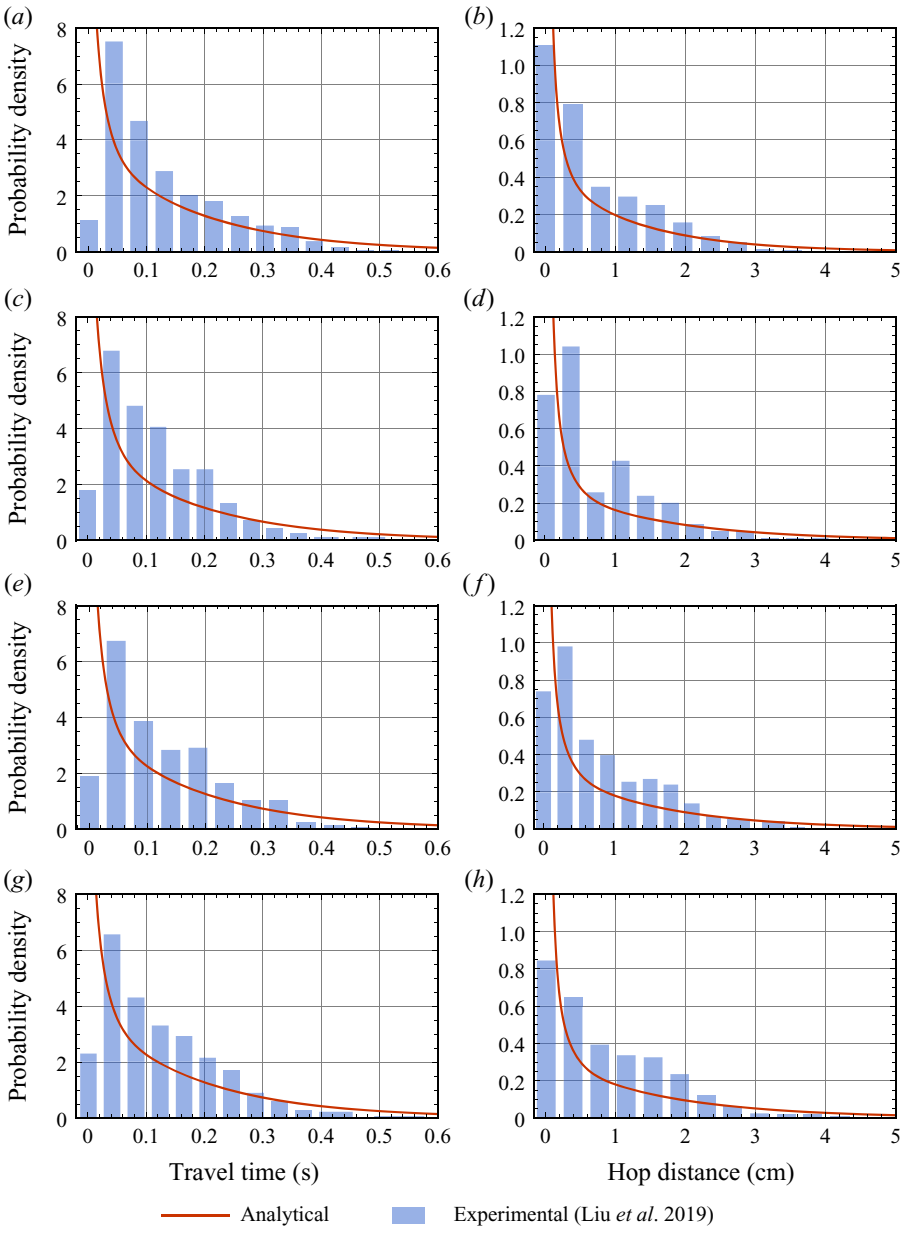

Figure 8. The p.d.f.s of (a,c,e,g) travel times f_T and (b,d,f,h) hop distances f_L for the four experimental groups of Liu *et al.* (2019). Experiments under flow rates from the low to high: S2 (a,b), S3 (c,d), S4 (e,f) and S5 (g,h).

validated by experimental observations with a quite different bedload particle diameter and transport conditions (Liu *et al.* 2019). To bridge the gap between the continuum model and the individual-based simulation, a deposition boundary condition for the governing FP equation is specified according to the numerical algorithm and experimental measurements for the first time. It is a simple Robin boundary condition, with an important parameter representing the deposition rate of bedload particles, which is similar to the

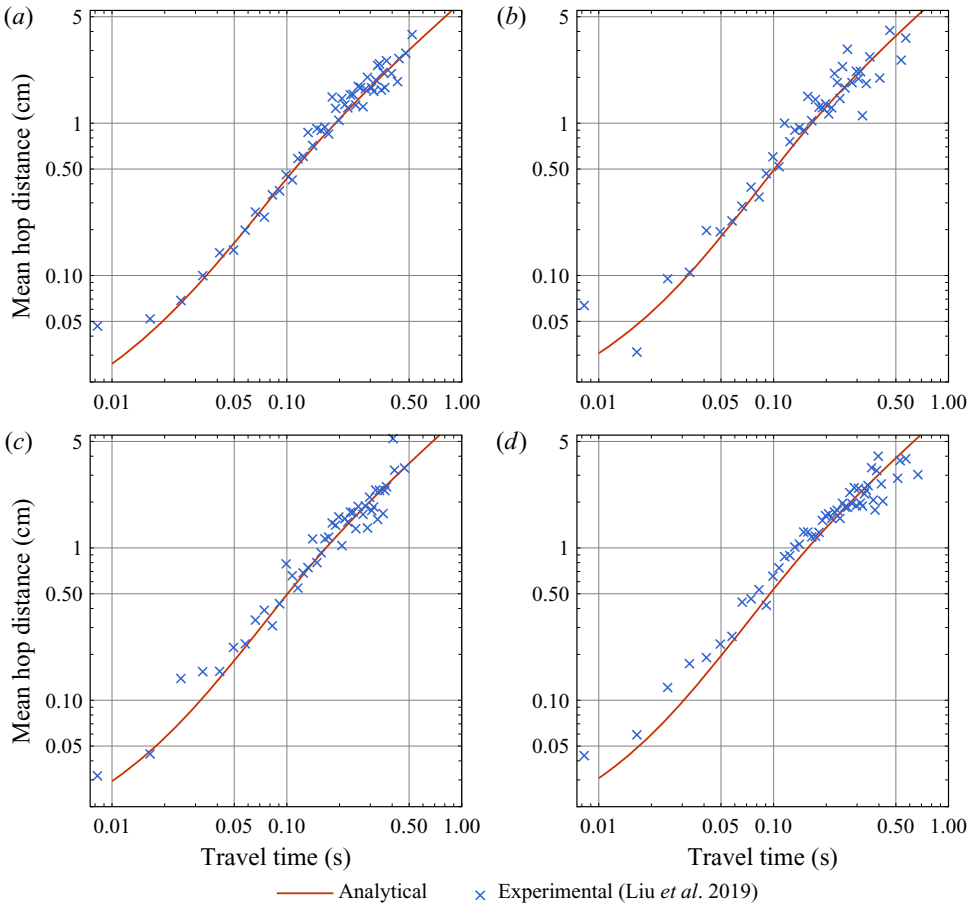

Figure 9. Mean hop distance over travel time $L(t)$ for the four experimental groups of Liu *et al.* (2019). Experiments under flow rates from the low to high: S2 (*a*), S3 (*b*), S4 (*c*) and S5 (*d*).

stopping chance for the numerical simulation. We have analytically shown that the newly introduced physical parameter of deposition rate is inversely proportional to the mean travel time or the mean hop distance, enabling a direct determination of the deposition rate based on the measured particle motion statistics. This is in contrast to the previous numerical simulation (Wu *et al.* 2020) using a fitting procedure matching the predicted quantities to the measurements for determining the stopping chance.

We have provided an analytical method to obtain theoretical results for particle hop statistics. The key is to treat the exponentially velocity-dependent diffusivity, which was determined by Wu *et al.* (2020) during a reanalysis of the experimental data (Fathel *et al.* 2015). We have devised a variable transformation such that the original bedload transport problem can be transformed into a simple problem of solute transport in laminar flow through a tube with a constant diffusivity. We can then directly use the classic analytical technique of Barton (1983) for solutions.

We have validated our analytical solutions using the numerical results of Wu *et al.* (2020), and the experimental results of Roseberry *et al.* (2012) (reanalysed by Fathel *et al.* 2015) and that of Liu *et al.* (2019). Then we investigate the influence of the deposition rate on three key characteristics of hop events: the p.d.f.s of travel times ($f_T(t)$) and hop

distances ($f_L(x)$), and the mean hop distance over travel time ($L(t)$), which are derived using the spatial and temporal moments with Taylor–Aris theory. It is found that a larger deposition rate can result in a longer mean hop distance over travel time, which can be counter-intuitive at first glance. From the limited experimental dataset under different flow rates, it is observed that the deposition frequency decreases as the shear stress increases when the flow rate is not small.

We emphasize that the theoretical framework of this present paper is different from the earlier work of Wu *et al.* (2021) mainly in the following two aspects. First, Wu *et al.* (2021) imposed a fundamental assumption on the pattern for the particle velocity variations (i.e. the particle is performing a Brownian motion in the stretched velocity dimension), which can be regarded as a certain simplification based on the general form of the FP equation (Furbish *et al.* 2012*b*). Instead, the present work directly used the general form of the FP equation with experimentally determined drift and diffusivity terms according to their definitions (Furbish *et al.* 2012*b*; Wu *et al.* 2020). No further simplification is required. Second, regarding the governing equations deduced in the two papers, the present work can describe the solute transport process in a tube flow (under a cylindrical coordinate system) as reflected by (3.4) and figure 2, while Wu *et al.* (2021) describes a process under a Cartesian coordinate system.

The FP equation proposed by Furbish *et al.* (2012*b*) is noted in this paper as a 'general form' in the sense that the forms of the drift and the diffusivity terms in the equation are open and can be arbitrary functions of the particle velocity based on experimental observations. Although specific forms have been used in the literature, including linear or constant drift and diffusivity, for example, the set of terms with a zero drift and an exponential form of diffusivity as presented in (2.2*a*,*b*) is one of the limited sets of results that have been directly determined based on the available experimental datasets of particle kinematics. This spells out the value of the present analytical work, while at the same time points out also the limitations and possible extensions in the future. For example, it remains to be seen how the forms of the two terms vary with the transport conditions, and if there exists a general form of the drift and diffusivity that can be applied to both subcritical and supercritical flows.

Regarding the velocity boundary condition for the governing FP equation, the deposition condition (2.5) is of the simplest possible form to account for the termination of bedload particle hops. Although this boundary condition is widely used in reactive transport problems, it may not be the most appropriate condition for bedload transport problems. As discussed in the results section, there is a noticeable deviation of both the analytical and numerical results from the experimental measurements for the p.d.f. of travel times at small values (figure 3), and in this region the curves for the analytical and numerical results decrease more quickly than the exponential distribution. This suggests that a modification to the deposition condition may be needed. Recently, Wu *et al.* (2021, (2.29)) applied a 'bulk' absorption term to the FP equation to account for the deposition, which means that bedload particles may have an equal chance of ceasing their motions at any velocity (Ancey *et al.* 2008; Ma *et al.* 2014; Wu *et al.* 2021; Pierce *et al.* 2022). Alternatives such as the time-fractional deposition process (Li *et al.* 2021) may also be considered.

Moreover, this work focuses only on the hop processes of the bedload particle transport. With the resting times taken into account, bedload particle transport across time scales can be analysed which contains multiple alternating processes of particle hops and rests (entrainment and deposition) (Parker, Paola & Leclair 2000; Garcia 2008; Ancey & Heyman 2014). And the p.d.f. of particle resting times is also closely related to the possible form of the boundary conditions. For example, some studies (Heyman *et al.* 2013) have

suggested an exponential distribution of resting times and thus a similar entrainment condition to the deposition condition (a Poisson process). As a comparison, there are other studies (Martin *et al.* 2012; Martin, Purohit & Jerolmack 2014; Fraccarollo & Hassan 2019; Liu *et al.* 2019; Pretzlav, Johnson & Bradley 2021) suggesting a power-law-like distribution for the resting times, although a simple form of the entrainment condition is not available yet. It is noted that, by incorporating other physical processes like the burial and exhumation of particles during their streamwise transport (Wu *et al.* 2019*a*,*b*), the power-law-like resting time distribution can be recovered which consequently induces the anomalous diffusion of bedload particles. Future theoretical work should therefore include an appropriate entrainment condition for bedload transport models.

Funding. This work was partially supported by the National Natural Science Foundation of China (U2243222, U2243240, 52179067, and 52109093) and the Fund Program of State key Laboratory of Hydroscience and Engineering (2022-KY-04). W.J. acknowledges the support of China Postdoctoral Science Foundation (2021M701906 and 2022T150362) and the Shuimu Tsinghua Scholar Program.

Declaration of interests. The authors report no conflict of interest.

Author ORCIDs.
Zi Wu https://orcid.org/0000-0003-1231-0893;
Weiquan Jiang https://orcid.org/0000-0002-2528-7736;
Li Zeng https://orcid.org/0000-0002-6547-2602;
Xudong Fu https://orcid.org/0000-0003-0744-0546.

Appendix A. Solution procedure for spatial and temporal moments

A.1. *Spatial moments for f_T and L*

Here, we solve the spatial moment μ_n for f_T and L in (3.7) and (3.9). First, according to the definition of moments (3.10*a*,*b*) and applying integration by parts to (3.4), we can obtain the initial-boundary-value problem for μ_n as

$$\frac{\partial \mu_n}{\partial t} - u(r)\mu_{n-1} = \frac{1}{r}\frac{\partial}{\partial r}\left(r\frac{\partial \mu_n}{\partial r}\right), \tag{A1a}$$

$$\left.\frac{\partial \mu_n}{\partial r}\right|_{r=1} = -\Gamma \mu_n|_{r=1}, \tag{A1b}$$

$$\mu_n|_{t=0} = \begin{cases} \frac{1}{2}\delta(r-1), & n=0, \\ 0, & n=1,2,\ldots, \end{cases} \tag{A1c}$$

for $n = 0, 1, 2, \ldots$ and $\mu_{-1} = \mu_{-2} = 0$.

Next, we can write the eigenvalue problem for (A1)

$$\frac{1}{r}\frac{\partial}{\partial r}\left(r\frac{\partial g}{\partial r}\right) = -\lambda g, \tag{A2a}$$

$$\left.\frac{\partial g}{\partial r}\right|_{r=1} = -\Gamma g|_{r=1}, \tag{A2b}$$

where λ is the eigenvalue to be solved, and $g(r)$ is the corresponding eigenfunction. Their solutions are

$$\lambda_i = \alpha_i^2, \quad g_i(r) = \frac{\alpha_i J_0(\alpha_i r)}{\sqrt{\alpha_i^2 + \Gamma^2} J_0(\alpha_i)}, \tag{A3a,b}$$

Index i	λ_i	a_i	ψ_i	b_i
0	2.171	0.487	1.552	0.338
1	17.647	0.663	14.964	−0.630
2	52.273	0.691	72.347	−0.506
3	180.608	0.702	106.569	−1.142
4	274.374	0.704	168.923	−0.737
5	387.877	0.705	270.245	−0.671

Table 3. The first few eigenvalues and coefficients of initial conditions for spatial and temporal moments.

where J_0 is the zeroth-order Bessel function of the first kind and $\{\lambda_i\}_{i=0}^{\infty}$ are the roots of

$$\alpha_i J_0'(\alpha_i) = -\Gamma J_0(\alpha_i). \tag{A4}$$

The first few eigenvalues are provided in table 3.

Here, $\{g_i(r)\}_{i=0}^{\infty}$ forms a basis for the function space satisfying the boundary condition (A1*b*).

For μ_0, from (2.8) of Barton (1984), we have

$$\mu_0(r,t) = \sum_{i=0}^{\infty} a_i \,\mathrm{e}^{-\lambda_i t} g_i(r), \tag{A5}$$

where coefficient a_i is related to the initial condition

$$a_i = \langle \mu_0(r, t=0), g_i(r)\rangle = \frac{\alpha_i}{2\sqrt{\alpha_i^2 + \Gamma^2}}, \quad i = 0, 1, \ldots, \tag{A6}$$

and the angle brackets define the inner product:

$$\langle f_1, f_2\rangle \triangleq \int_0^1 r f_1(r) f_2(r)\,\mathrm{d}r, \tag{A7}$$

where $f_1(r)$ and $f_2(r)$ are arbitrary functions. The values of the first few a_i are presented in table 3.

For μ_1, by (2.9) of Barton (1984) we have

$$\mu_1(r,t) = \sum_{i=0}^{\infty} a_i B_{i,i} t\,\mathrm{e}^{-\lambda_i t} g_i(r) + \sum_{\substack{i,j=0\\ j\neq i}}^{\infty} \frac{a_j B_{i,j}(\mathrm{e}^{-\lambda_j t} - \mathrm{e}^{-\lambda_i t})}{\lambda_i - \lambda_j} g_i(r), \tag{A8}$$

where coefficient $B_{i,j}$ is related to $u(r)$ and can be calculated as

$$B_{i,j} = \langle u(r) g_i(r), g_j(r)\rangle = \langle -2\ln r g_i(r), g_j(r)\rangle, \tag{A9}$$

for $i, j = 0, 1, \ldots$.

A.2. *Temporal moments for f_L*

Here, we solve the temporal moment m_0 for f_L in (3.8). First, according to the definition (3.10*a*,*b*) and applying the integration by parts to (3.4), the governing equation of m_n is

$$-\delta_{0n}c|_{t=0} - nm_{n-1} + u(r)\frac{\partial m_n}{\partial x} = \frac{1}{r}\frac{\partial}{\partial r}\left(r\frac{\partial m_n}{\partial r}\right), \tag{A10}$$

for $n = 0, 1, 2, \ldots$ and δ_{ij} is the Kronecker delta. The boundary condition of m_n is in the same form as (3.4*b*).

Note that in the initial condition (3.4*c*), c_{init} is a Dirac delta function of x. Therefore, we can rewrite the problem of m_n as

$$\frac{\partial m_n}{\partial x} - \frac{1}{u(r)}nm_{n-1} = \frac{1}{u(r)}\frac{1}{r}\frac{\partial}{\partial r}\left(r\frac{\partial m_n}{\partial r}\right), \tag{A11a}$$

$$\left.\frac{\partial m_n}{\partial r}\right|_{r=1} = -\Gamma m_n|_{r=1}, \tag{A11b}$$

$$m_n|_{x=0} = \begin{cases} \dfrac{1}{2u(r)}\delta(r-1), & n = 0, \\ 0, & n = 1, 2, \ldots. \end{cases} \tag{A11c}$$

Now we can see that the above initial-boundary-value problem of m_n is very similar to (A1) of μ_n, and we can also use the method of Barton (1983, 1984) for the analytical solution.

The corresponding eigenvalue problem for (A11) is

$$\frac{1}{u(r)}\frac{1}{r}\frac{\partial}{\partial r}\left(r\frac{\partial h}{\partial r}\right) = -\psi h, \tag{A12a}$$

$$\left.\frac{\partial h}{\partial r}\right|_{r=1} = -\Gamma h|_{r=1}, \tag{A12b}$$

where ψ is the eigenvalue and $h(r)$ is its eigenfunction. The inner product is defined as

$$\langle f_1, f_2\rangle_T \triangleq \int_0^1 ru(r)f_1(r)f_2(r)\,\mathrm{d}r, \tag{A13}$$

where $f_1(r)$ and $f_2(r)$ are arbitrary functions.

Suppose we have found a sequence of solution of eigenvalues, denoted as $\{\psi_i\}_{i=0}^{\infty}$, and the corresponding eigenfunctions $\{h_i\}_{i=0}^{\infty}$. Then, similar to (A5), by (2.8) of Barton (1984), we have

$$m_0(x, r) = \sum_{i=0}^{\infty} b_i\,\mathrm{e}^{-\psi_i x}h_i(r), \tag{A14}$$

where the coefficient b_i is

$$b_i = \langle m_0(x = 0, r), h_i(r)\rangle_T = \frac{h_i(1)}{2}, \quad i = 0, 1, \ldots. \tag{A15}$$

The values of the first few b_i are presented in table 3.

Next, we solve the eigenvalue problem (A12) by the GITT method (Cotta 1993; Rubol, Battiato & de Barros 2016; Guo & Chen 2022) because the diffusion term contains $u(r)$,

which makes it more complicated than (A2). Fortunately, we can use the function basis $\{g_i(r)\}_{i=0}^{\infty}$ by (A2), and perform a series expansion for $h_i(r)$ using the GITT method

$$h_i(r) = \sum_{j=0}^{\infty} \eta_{ij} g_j(r), \quad i = 0, 1, \ldots, \tag{A16}$$

where η_{ij} is the expansion coefficient. We can also express the results in the matrix form. Defining $\boldsymbol{\eta}_i = (\eta_{i0}, \eta_{i1}, \cdots)^{\mathrm{T}}$ and $\boldsymbol{g} = (g_0, g_1, \cdots)^{\mathrm{T}}$, then $h_i = \boldsymbol{\eta}_i^{\mathrm{T}} \boldsymbol{g}$, where T denotes the transpose. Performing the integral transform for (A12*a*), we obtain the linear equation for the coefficient vector $\boldsymbol{\eta}$

$$\boldsymbol{A}\boldsymbol{\eta}_i = \psi_i \boldsymbol{\eta}_i, \tag{A17}$$

where the elements of matrix $\boldsymbol{A}$ are

$$A_{ij} = \left\langle g_i, \frac{1}{u(r)} \frac{1}{r} \frac{\partial}{\partial r} \left(r \frac{\partial g_j}{\partial r} \right) \right\rangle_T. \tag{A18}$$

Therefore, ψ_i is the eigenvalue of $\boldsymbol{A}$ and $\boldsymbol{\eta}_i$ is the corresponding eigenvector, which can be obtained after a truncation for the series expansion (A16) to some degree. The first few ψ_i are presented in table 3. Finally, we remark that one can also apply the GITT method directly to (A10) and thus expand m_0 with the function basis $\{g_i(r)\}_{i=0}^{\infty}$. A similar solution procedure was presented in the work of Rubol *et al.* (2016, (12)).

Appendix B. Solution for universal moments

According to the definition (4.3) of the universal moment, the governing equations for $M_{n,m}$ can be obtain by applying the integration by parts to (A1) or (A10)

$$-\delta_{0m}\mu_n|_{t=0} - M_{n,m-1} - u(r)M_{n-1,m} = \frac{1}{r}\frac{\partial}{\partial r}\left(r \frac{\partial M_{n,m}}{\partial r} \right), \tag{B1a}$$

$$\left. \frac{\partial M_{n,m}}{\partial r} \right|_{r=1} = -\Gamma M_{n,m}|_{r=1}, \tag{B1b}$$

for $n = 0, 1, 2, \ldots$ and $m = 0, 1, 2, \ldots$. Here, $M_{-1,0}$, $M_{-1,-1}$ and $M_{0,-1}$ all equal to zero. By calculating the cross-sectional mean of $M_{n,m}$ with respect to r, which is

$$\bar{M}_{n,m} = \int_0^1 2r M_{n,m}(r)\, \mathrm{d}r, \tag{B2}$$

we immediately have

$$-\delta_{0m}\overline{\mu_n}|_{t=0} - \bar{M}_{n,m-1} - \overline{u(r)M_{n-1,m}} = 2\Gamma M_{n,m}|_{r=1}. \tag{B3}$$

According to (4.1) and (4.2), the mean travel time T_a and the mean hop distance L_a are related to $M_{0,1}$ and $M_{1,0}$, respectively. Now with (B3), we have

$$T_a = 2\Gamma M_{0,1}|_{r=1} = \bar{M}_{0,0}, \quad L_a = 2\Gamma M_{1,0}|_{r=1} = \overline{-u(r)M_{0,0}}. \tag{B4a,b}$$

Therefore, we only need to solve $M_{0,0}$.

By (B1*a*), the governing equation of $M_{0,0}$ is

$$-\mu_0|_{t=0} = \frac{1}{r}\frac{\partial}{\partial r}\left(r\frac{\partial M_{0,0}}{\partial r}\right). \tag{B5}$$

Its general solution can be written as

$$M_{0,0} = \int_0^r \frac{1}{r''}\left(\int_0^{r''} -r'\mu_0(r, t=0)\,\mathrm{d}r' + A\right)\mathrm{d}r'' + B, \tag{B6}$$

where A and B are undetermined constants. Note that $A = 0$ because $\ln r|_{r=0} = -\infty$. And the initial condition (A1*c*) of μ_0 is a delta function. Therefore,

$$\begin{aligned} M_{0,0}(r) &= \int_0^r \frac{1}{r''}\left(\int_0^{r''} -r'\mu_0(r, t=0)\,\mathrm{d}r'\right)\mathrm{d}r'' + B \\ &= -\int_0^r \frac{1}{r''}\frac{H(r''-1)}{2}\,\mathrm{d}r'' + B \\ &= -\frac{1}{2}H(r-1)\ln r + B, \end{aligned} \tag{B7}$$

where $H(r)$ is the Heaviside step function. According to the boundary condition (B1*b*), we have

$$-\tfrac{1}{2} = -\Gamma B, \tag{B8}$$

namely $B = 1/(2\Gamma)$.

Appendix C. Deposition condition with a cutoff velocity

If one imposes the cutoff velocity to determine the resting state, then the deposition condition for the bedload particle hops should be modified, as presented in (5.2). The initial condition (2.4) also needs modification

$$P^*_{init} = \delta(x^*)\delta(u^* - u^*_c). \tag{C1}$$

To handle the cutoff velocity, we impose the velocity translation, $u'^* = u^* - u^*_c$. Then, with a modified velocity diffusion coefficient

$$k'^*_0 \triangleq k^*_0\,\mathrm{e}^{u^*_c/u^*_0}, \tag{C2}$$

the transformed bedload transport problem,

$$\frac{\partial P^*}{\partial t^*} + \left(u'^* + u^*_c\right)\frac{\partial P^*}{\partial x^*} = \frac{\partial^2}{\partial u'^{*2}}(k'^*_0\,\mathrm{e}^{u'^*/u^*_0}P^*), \tag{C3a}$$

$$k'^*_0\left.\frac{\partial P^*}{\partial u'^*}\right|_{u'^*=0} = \Gamma^* P^*|_{u'^*=0}, \tag{C3b}$$

$$P^*_{init} = \delta(x^*)\delta(u'^*), \tag{C3c}$$

is nearly in the same form as the original one (2.3)–(2.5), with only a slight difference in the advection term. Therefore, we can still use the dimensionless variables and parameters in (3.1), and then introduce the transformation for the exponential diffusivity term in

(3.3*a*,*b*), replacing u^* and k_0^* with $u'*$ and $k_0'^*$, respectively. We can change the advective term in (3.4*a*) to have

$$\frac{\partial c}{\partial t} + [u'(r) + u_c]\frac{\partial c}{\partial x} = \frac{1}{r}\frac{\partial}{\partial r}\left(r\frac{\partial c}{\partial r}\right), \tag{C4}$$

where the dimensionless cutoff velocity $u_c = u_c^*/u_0^*$. In fact, we can also keep using the original transport problem for c with a different definition for the 'velocity profile' $u(r) = -2\ln r + u_c$. Then the analytical solution procedure for the spatial and temporal moments are exactly the same.

We have the following results for the hop statistics. First, the p.d.f. of particle velocities under the equilibrium transport conditions now becomes

$$f_U^*(u^*) = \frac{1}{u_0^*}\,\mathrm{e}^{-(u^*-u_c^*)/u_0^*}, \tag{C5}$$

and thus $\int_{u_c^*}^{\infty} f_U^*(u^*)\,\mathrm{d}u^* = 1$. The average velocity is

$$\frac{L_a^*}{T_a^*} = u_a^* = \int_{u_c^*}^{\infty} u^* f_U^*(u^*)\,\mathrm{d}u^* = u_0^* + u_c^*. \tag{C6}$$

For the average travel time and average hop distance, the relationship (4.6) is changed to

$$T_a^* = \frac{u_0^*}{\Gamma^*} = \frac{u_a^* - u_c^*}{\Gamma^*}, \tag{C7a}$$

$$L_a^* = u_a^* T_a^* = (u_0^* + u_c^*)\frac{u_0^*}{\Gamma^*}. \tag{C7b}$$

Appendix D. Acceleration distribution

We can use the Euler–Maruyama scheme for discrete SDEs to approximate the p.d.f. of accelerations with a small time step. First, the Euler–Maruyama approximation of (2.1*b*) is

$$A \approx \frac{\Delta U}{\Delta t^*} \approx \frac{\sqrt{2k^*(U)\Delta t^*}\,\Delta\xi^*}{\Delta t} \tag{D1}$$

where A is the random variable of acceleration a^*, U is the random variable of velocity u^* and $\Delta\xi^* \sim N(0, 1)$ follows the standard normal distribution. The time step Δt^* should be small enough (Miao *et al.* 2018).

Next, we write A^* as a product of three factors

$$A = \sqrt{\frac{2k_0^*}{\Delta t^*}}A_1A_2 = \sqrt{\frac{2k_0^*}{\Delta t^*}}Z, \tag{D2}$$

where $Z = A_1A_2$,

$$A_1(U) = \sqrt{\frac{k^*(U)}{k_0^*}} = \mathrm{e}^{U/2u_0^*}, \tag{D3}$$

and $A_2 = \Delta\xi^*$. Note that A_1 is a function U and $U \sim Exp(1/u_0^*)$ follows an exponential distribution (because the velocity distribution is exponential Wu *et al.* 2020). With the

inverse function $U(A_1) = 2u_0^* \ln(A_1)$, the p.d.f. of A_1 is

$$f_{A_1}(a_1) = f_U^*[u^*(a_1)] \left| \frac{\mathrm{d}U}{\mathrm{d}A_1} \right| \tag{D4}$$

$$= \frac{1}{u_0^*} \exp\left(-\frac{u^*(a_1)}{u_0^*} \right) \left| \frac{2u_0^*}{a_1} \right| \tag{D5}$$

$$= \frac{1}{u_0^*} \exp\left(-\frac{2u_0^* \ln a_1}{u_0^*} \right) \left| \frac{2u_0^*}{a_1} \right| \tag{D6}$$

$$= \frac{1}{u_0^*} \frac{1}{a_1^2} \left| \frac{2u_0^*}{a_1} \right| \tag{D7}$$

$$= \frac{2}{a_1^3}. \tag{D8}$$

The p.d.f. of A_2 is Gaussian,

$$f_{A_2}(a_2) = \frac{1}{\sqrt{2\pi}} \exp\left(-\frac{a_2^2}{2} \right). \tag{D9}$$

According to rules for the joint p.d.f. of the product of two independent random variables, for $Z = A_1 A_2$, we have

$$f_Z(z) = f_{A_1 A_2}(z) = \int_{-\infty}^{\infty} \frac{1}{|a_2|} f_{A_2}(a_2) f_{A_1}\left(\frac{z}{a_2} \right) \mathrm{d}a_2. \tag{D10}$$

Note that $A_1 \in [1, +\infty)$, then

$$f_{A_1 A_2}(z) = \int_{-z}^{z} \frac{1}{\sqrt{2\pi}} \mathrm{e}^{-a_2^2/2} \frac{1}{|a_2|} \left(\frac{2a_2^3}{z^3} \right) \mathrm{d}a_2. \tag{D11}$$

For $z > 0$, we have

$$\begin{aligned} f_{A_1 A_2}(z) &= \int_0^z \frac{1}{\sqrt{2\pi}} \mathrm{e}^{-a_2^2/2} \frac{1}{|a_2|} \left(\frac{2a_2^3}{z^3} \right) \mathrm{d}a_2 \\ &= \frac{2}{\sqrt{2\pi}} \frac{1}{z^3} \int_0^z a_2^2 \mathrm{e}^{-a_2^2/2} \, \mathrm{d}a_2 \\ &= \frac{2}{\sqrt{2\pi}} \frac{1}{z^3} \left[-z \mathrm{e}^{-z^2/2} + \sqrt{\frac{\pi}{2}} \, Erf\left(\frac{z}{\sqrt{2}} \right) \right] \\ &= \frac{1}{z^3} Erf\left(\frac{z}{\sqrt{2}} \right) - \frac{\sqrt{2}}{\sqrt{\pi}} \frac{1}{z^2} \mathrm{e}^{-z^2/2}, \end{aligned} \tag{D12}$$

where *Erf* is the error function. Note that $f_Z(z)$ is an even function. Finally, for the acceleration in (D2), we just need to put in the constant factor $\sqrt{2k_0^*/\Delta t^*}$

$$f_A(a^*) = \frac{1}{\sqrt{2k_0^*/\Delta t^*}} f_{A_1 A_2}\left(\frac{a^*}{\sqrt{2k_0^*/\Delta t^*}} \right). \tag{D13}$$

Note that the above approximated form for the p.d.f. of acceleration is complicated. In practice, the simple Laplace distribution ($Laplace(0, b)$) is a more common choice for

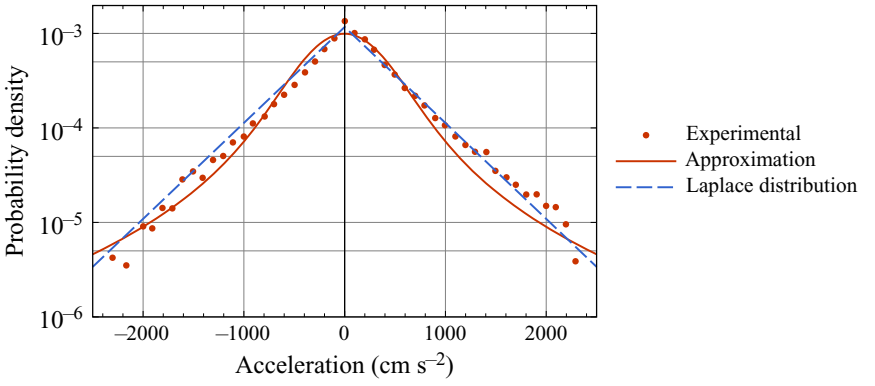

Figure 10. Comparison of p.d.f. of acceleration for experiment S5 of Liu *et al.* (2019). 'Approximation' represents the solution by (D13).

approximation (Wu *et al.* 2020). As shown in figure 10, the Laplace distribution even gives a better prediction than that by the numerical approximation (D13). The mean of the absolute of acceleration (mean absolute deviation, a^*_{mad}) or the standard deviation of acceleration (a^*_{std}) is useful for the estimation of the parameter b. Using the property of independent distributions, we have

$$\begin{aligned} a^*_{mad} = \mu_{|A|} &= \sqrt{\frac{2k_0^*}{\Delta t^*}}\mu_{|A_2|}\mu_{|A_1|} \\ &= \sqrt{\frac{2k_0^*}{\Delta t^*}}\left[\int_0^\infty \sqrt{\frac{k(u^*)}{k_0^*}} f_U^*(u^*)\,\mathrm{d}u^*\right]\left[2\int_0^\infty a_2 \frac{1}{\sqrt{2\pi}}\,\mathrm{e}^{-a_2^2/2}\,\mathrm{d}a_2\right] \\ &= \sqrt{\frac{2k_0^*}{\Delta t^*}}\left(\int_0^\infty \mathrm{e}^{u^*/2u_0^*}\frac{1}{u_0^*}\,\mathrm{e}^{-u^*/u_0^*}\,\mathrm{d}u^*\right)2\frac{1}{\sqrt{2\pi}} \\ &= 4\sqrt{\frac{k_0^*}{\pi\Delta t^*}}. \end{aligned} \tag{D14}$$

Note that the mean absolute deviation of $Laplace(0, b)$ is b and thus

$$b = 4\sqrt{\frac{k_0^*}{\pi\Delta t^*}}. \tag{D15}$$

If one uses the standard deviation of acceleration, note that the standard deviation of A_1 does not exist probably because (D1) is only a first-order approximation. Thus, we have to use the Laplace distribution as an approximation and the variance $(a^*_{std})^2 = 2b^2$. Together with (D15), we have

$$k_0^* = \tfrac{1}{32}\pi\Delta t^*(a^*_{std})^2. \tag{D16}$$

Finally, if one imposes the cutoff velocity, the analysis is similar after we make the translation $u'^* = u^* - u_c^*$, as presented in § C. We just need to replace u^* and k_0^* in (D14) with u'^* and $k_0'^*$ (defined in (C2)), respectively. Then, (D16) is generalized for the presence of the cutoff velocity as

$$k_0^*\,\mathrm{e}^{u_c^*/u_0^*} = k_0'^* = \tfrac{1}{32}\pi\Delta t^*(a^*_{std})^2. \tag{D17}$$

References

Ancey, C. 2020 Bedload transport: a walk between randomness and determinism. Part 1. The state of the art. *J. Hydraul Res.* **58** (1), 1–17.

Ancey, C., Davison, A.C., Böhm, T., Jodeau, M. & Frey, P. 2008 Entrainment and motion of coarse particles in a shallow water stream down a steep slope. *J. Fluid Mech.* **595**, 83–114.

Ancey, C. & Heyman, J. 2014 A microstructural approach to bed load transport: mean behaviour and fluctuations of particle transport rates. *J. Fluid Mech.* **744**, 129–168.

Andrews, S.S. 2009 Accurate particle-based simulation of adsorption, desorption and partial transmission. *Phys. Biol.* **6** (4), 046015.

Aris, R. 1956 On the dispersion of a solute in a fluid flowing through a tube. *Proc. R. Soc. Lond. Math. Phys. Engng Sci.* **235** (1200), 67–77.

Barton, N.G. 1983 On the method of moments for solute dispersion. *J. Fluid Mech.* **126**, 205–218.

Barton, N.G. 1984 An asymptotic theory for dispersion of reactive contaminants in parallel flow. *J. Austral. Math. Soc. Ser. B Appl. Math.* **25** (3), 287–310.

Cherstvy, A.G. & Metzler, R. 2013 Population splitting, trapping, and non-ergodicity in heterogeneous diffusion processes. *Phys. Chem. Chem. Phys.* **15** (46), 20220–20235.

Chien, N. & Wan, Z. 1999 *Mechanics of Sediment Transport*. American Society of Civil Engineers.

Cotta, R.M. 1993 *Integral Transforms in Computational Heat and Fluid Flow*. CRC Press.

Debnath, S., Jiang, W., Guan, M. & Chen, G. 2022 Effect of ring-source release on dispersion process in Poiseuille flow with wall absorption. *Phys. Fluids* **34** (2), 027106.

Einstein, H.A. 1936 Der Geschiebetrieb als Wahrscheinlichkeitsproblem (Bedload transport as a probability problem). PhD thesis, ETH Zurich, Zurich.

Einstein, H.A. 1942 Formulas for the transportation of bed load. *Trans. Am. Soc. Civ. Engrs* **107** (1), 561–577.

Einstein, H.A. 1950 The bed-load function for sediment transportation in open channel flows. *Tech. Rep.* 1026. United States Department of Agriculture.

Erban, R. & Chapman, S.J. 2007 Reactive boundary conditions for stochastic simulations of reaction–diffusion processes. *Phys. Biol.* **4** (1), 16–28.

Fan, N., Singh, A., Guala, M., Foufoula-Georgiou, E. & Wu, B. 2016 Exploring a semimechanistic episodic langevin model for bed load transport: emergence of normal and anomalous advection and diffusion regimes. *Water Resour. Res.* **52** (4), 2789–2801.

Fan, N., Zhong, D., Wu, B., Foufoula-Georgiou, E. & Guala, M. 2014 A mechanistic-stochastic formulation of bed load particle motions: from individual particle forces to the Fokker-Planck equation under low transport rates. *J. Geophys. Res. Earth Surf.* **119** (3), 464–482.

Fathel, S.L., Furbish, D.J. & Schmeeckle, M.W. 2015 Experimental evidence of statistical ensemble behavior in bed load sediment transport. *J. Geophys. Res. Earth Surf.* **120** (11), 2298–2317.

Fraccarollo, L. & Hassan, M.A. 2019 Einstein conjecture and resting-time statistics in the bed-load transport of monodispersed particles. *J. Fluid Mech.* **876**, 1077–1089.

Furbish, D.J., Haff, P.K., Roseberry, J.C. & Schmeeckle, M.W. 2012*a* A probabilistic description of the bed load sediment flux: 1. Theory. *J. Geophys. Res. Earth Surf.* **117** (F3), F03031.

Furbish, D.J., Roseberry, J.C. & Schmeeckle, M.W. 2012*b* A probabilistic description of the bed load sediment flux: 3. The particle velocity distribution and the diffusive flux. *J. Geophys. Res. Earth Surf.* **117** (F3), F03033.

Garcia, M. 2008 Sediment transport and morphodynamics. In *Sedimentation Engineering: Processes, Measurements, Modeling, and Practice*, pp. 21–163. American Society of Civil Engineers.

Guan, M.Y., Zeng, L., Jiang, W.Q., Guo, X.L., Wang, P., Wu, Z., Li, Z. & Chen, G.Q. 2022 Effects of wind on transient dispersion of active particles in a free-surface wetland flow. *Commun. Nonlinear Sci. Numer. Simul.* **115**, 106766.

Guo, J. & Chen, G. 2022 Solute dispersion from a continuous release source in a vegetated flow: an analytical study. *Water Resour. Res.* **58** (4), e2021WR030255.

Harvey, C.F. & Gorelick, S.M. 1995 Temporal moment-generating equations: modeling transport and mass transfer in heterogeneous aquifers. *Water Resour. Res.* **31** (8), 1895–1911.

Heyman, J., Bohorquez, P. & Ancey, C. 2016 Entrainment, motion, and deposition of coarse particles transported by water over a sloping mobile bed. *J. Geophys. Res. Earth Surf.* **121** (10), 1931–1952.

Heyman, J., Mettra, F., Ma, H.B. & Ancey, C. 2013 Statistics of bedload transport over steep slopes: separation of time scales and collective motion. *Geophys. Res. Lett.* **40** (1), 128–133.

Jiang, W.Q. & Chen, G.Q. 2018 Solution of Gill's generalized dispersion model: solute transport in Poiseuille flow with wall absorption. *Intl J. Heat Mass Transfer* **127**, 34–43.

Jiang, W., Zeng, L., Fu, X. & Wu, Z. 2022 Analytical solutions for reactive shear dispersion with boundary adsorption and desorption. *J. Fluid Mech.* **947**, A37.

KALINSKE, A.A. 1947 Movement of sediment as bed load in rivers. *Eos Trans. Am. Geophys. Union* **28** (4), 615–620.

KOWALL, J., PEAK, D. & CORBETT, J.W. 1976 Impurity-concentration profile for an exponentially decaying diffusion coefficient in irradiation enhanced diffusion. *Phys. Rev.* B **13** (2), 477–478.

LAJEUNESSE, E., MALVERTI, L. & CHARRU, F. 2010 Bed load transport in turbulent flow at the grain scale: experiments and modeling. *J. Geophys. Res. Earth Surf.* **115** (F4), F04001.

LI, Z., CHEN, D., SUN, H., MENG, Z., ZHANG, Y. & SIBATOV, R.T. 2021 Analyzing and modeling sub-diffusive transport of bedload along a heterogeneous gravel bed using stochastic and statistical methods. *J. Hydrol.* **596**, 125697.

LI, G., JIANG, W., WANG, P., GUO, J., LI, Z. & CHEN, G.Q. 2018 Concentration moments based analytical study on Taylor dispersion: open channel flow driven by gravity and wind. *J. Hydrol.* **562**, 244–253.

LIU, M.X., PELOSI, A. & GUALA, M. 2019 A statistical description of particle motion and rest regimes in open-channel flows under low bedload transport. *J. Geophys. Res. Earth Surf.* **124** (11), 2666–2688.

MA, H., HEYMAN, J., FU, X., METTRA, F., ANCEY, C. & PARKER, G. 2014 Bed load transport over a broad range of timescales: determination of three regimes of fluctuations. *J. Geophys. Res. Earth Surf.* **119** (12), 2653–2673.

MABY, E.W. 1976 Bombardment-enhanced diffusion of arsenic in silicon. *J. Appl. Phys.* **47** (3), 830–836.

MARTIN, R.L., JEROLMACK, D.J. & SCHUMER, R. 2012 The physical basis for anomalous diffusion in bed load transport. *J. Geophys. Res. Earth Surf.* **117** (F1), F01018.

MARTIN, R.L., PUROHIT, P.K. & JEROLMACK, D.J. 2014 Sedimentary bed evolution as a mean-reverting random walk: implications for tracer statistics. *Geophys. Res. Lett.* **41** (17), 6152–6159.

MIAO, W., CAO, L., ZHONG, Q. & LI, D. 2018 Influence of the time interval on image-based measurement of bed-load transport. *J. Hydraul. Res.* **56** (4), 567–575.

PARKER, G., PAOLA, C. & LECLAIR, S. 2000 Probabilistic Exner sediment continuity equation for mixtures with no active layer. *ASCE J. Hydraul. Engng* **126** (11), 818–826.

PIERCE, J.K., HASSAN, M.A. & FERREIRA, R.M.L. 2022 Probabilistic description of bedload fluxes from the aggregate dynamics of individual grains. *Earth Surf. Dyn.* **10** (4), 817–832.

PRETZLAV, K.L.G., JOHNSON, J.P.L. & BRADLEY, D.N. 2021 Smartrock transport from seconds to seasons: shear stress controls on gravel diffusion inferred from hop and rest scaling. *Geophys. Res. Lett.* **48** (9), e2020GL091991.

ROSEBERRY, J.C., SCHMEECKLE, M.W. & FURBISH, D.J. 2012 A probabilistic description of the bed load sediment flux: 2. Particle activity and motions. *J. Geophys. Res. Earth Surf.* **117** (F3), F03032.

RUBOL, S., BATTIATO, I. & DE BARROS, F.P.J. 2016 Vertical dispersion in vegetated shear flows. *Water Resour. Res.* **52** (10), 8066–8080.

SINGER, A., SCHUSS, Z., OSIPOV, A. & HOLCMAN, D. 2008 Partially reflected diffusion. *SIAM J. Appl. Maths* **68** (3), 844–868.

TAYLOR, G. 1953 Dispersion of soluble matter in solvent flowing slowly through a tube. *Proc. R. Soc. Lond. Math. Phys. Engng Sci.* **219** (1137), 186–203.

WANG, P. & CHEN, G.Q. 2017 Basic characteristics of Taylor dispersion in a laminar tube flow with wall absorption: exchange rate, advection velocity, dispersivity, skewness and kurtosis in their full time dependance. *Intl J. Heat Mass Transfer* **109**, 844–852.

WANG, W., CHERSTVY, A.G., LIU, X. & METZLER, R. 2020 Anomalous diffusion and nonergodicity for heterogeneous diffusion processes with fractional Gaussian noise. *Phys. Rev.* E **102** (1), 012146.

WANG, B., JIANG, W. & CHEN, G. 2022*a* Gyrotactic trapping of micro-swimmers in simple shear flows: a study directly from the fundamental Smoluchowski equation. *J. Fluid Mech.* **939**, A37.

WANG, B., JIANG, W., CHEN, G. & TAO, L. 2022*b* Transient dispersion in a channel with crossflow and wall adsorption. *Phys. Rev. Fluids* **7** (7), 074501.

WU, Z., FOUFOULA-GEORGIOU, E., PARKER, G., SINGH, A., FU, X. & WANG, G. 2019*a* Analytical solution for anomalous diffusion of bedload tracers gradually undergoing burial. *J. Geophys. Res. Earth Surf.* **124** (1), 21–37.

WU, Z., FURBISH, D. & FOUFOULA-GEORGIOU, E. 2020 Generalization of hop distance-time scaling and particle velocity distributions via a two-regime formalism of bedload particle motions. *Water Resour. Res.* **56** (1), e2019WR025116.

WU, Z., SINGH, A., FOUFOULA-GEORGIOU, E., GUALA, M., FU, X. & WANG, G. 2021 A velocity-variation-based formulation for bedload particle hops in rivers. *J. Fluid Mech.* **912**, A33.

WU, Z., SINGH, A., FU, X. & WANG, G. 2019*b* Transient anomalous diffusion and advective slowdown of bedload tracers by particle burial and exhumation. *Water Resour. Res.* **55** (10), 7964–7982.

ZENG, L., CHEN, G.Q., TANG, H.S. & WU, Z. 2011 Environmental dispersion in wetland flow. *Commun. Nonlinear Sci. Numer. Simul.* **16** (1), 206–215.